

A Two Micron All-Sky Survey View of the Sagittarius Dwarf Galaxy:

VI. s-Process and Titanium Abundance Variations Along the Sagittarius Stream

Mei-Yin Chou¹, Katia Cunha^{2,3}, Steven R. Majewski¹, Verne V. Smith²,
Richard J. Patterson¹, David Martínez-Delgado⁴ and Doug Geisler⁵

ABSTRACT

We present high-resolution spectroscopic measurements of the abundances of the α element titanium (Ti) and s-process elements yttrium (Y) and lanthanum (La) for 59 candidate M giant members of the Sagittarius (Sgr) dwarf spheroidal (dSph) + tidal tail system pre-selected on the basis of position and radial velocity. As expected, the majority of these stars show peculiar abundance patterns compared to those of nominal Milky Way stars, but as a group the stars form a coherent picture of chemical enrichment of the Sgr dSph from $[\text{Fe}/\text{H}] = -1.4$ to solar abundance. This sample of spectra provides the largest number of Ti, La and Y abundances yet measured for a dSph, and spans metallicities not typically probed by studies of the other, generally more metal-poor Milky Way (MW) satellites. On the other hand, the overall $[\text{Ti}/\text{Fe}]$, $[\text{Y}/\text{Fe}]$, $[\text{La}/\text{Fe}]$ and $[\text{La}/\text{Y}]$ patterns with $[\text{Fe}/\text{H}]$ of the Sgr stream plus Sgr core do, for the most part, resemble those seen in the Large Magellanic Cloud (LMC) and other dSphs, only shifted by $\Delta[\text{Fe}/\text{H}] \sim +0.4$ from the LMC and by $\sim +1$ dex from the other dSphs; these relative shifts reflect the faster and/or more efficient chemical evolution of Sgr compared to the other satellites, and show that Sgr has had an enrichment history more like the LMC than the other dSphs. By tracking the evolution of the abundance patterns along the Sgr stream we can follow the time variation of

¹Dept. of Astronomy, University of Virginia, Charlottesville, VA 22904-4325 (mc6ss, srm4n, rjp0i@virginia.edu)

²National Optical Astronomy Observatories, PO Box 26732, Tucson, AZ 85726 (cunha, vsmith@noao.edu)

³On leave from Observatorio Nacional, Rio de Janeiro, Brazil

⁴Instituto de Astrofísica de Canarias, La Laguna, Spain (ddelgado@iac.es)

⁵Departamento de Astronomía, Universidad de Concepción, Casilla 160-C, Concepción, Chile (dgeisler@astro-udec.cl)

the chemical make-up of dSph stars donated to the Galactic halo by Sgr. This evolution demonstrates that while the bulk of the stars currently in the Sgr dSph are quite unlike those of the Galactic halo, an increasing number of stars farther along the Sgr stream have abundances like Milky Way halo stars, a trend that shows clearly how the Galactic halo could have been contributed by present day satellite galaxies even if the *present* chemistry of those satellites is now different from typical halo field stars. Finally, we analyze the chemical abundances of a moving group of M giants among the Sgr leading arm stars at the North Galactic Cap, but having radial velocities unlike the infalling Sgr leading arm debris there. Through use of “chemical fingerprinting”, we conclude that these mostly receding northern hemisphere M giants also are Sgr stars, likely *trailing arm* debris overlapping the Sgr leading arm in the north.

Subject headings: galaxies: evolution – galaxies: interactions – Galaxy: halo – Galaxy: abundances – galaxies: individual: Sagittarius dSph – stars: abundances

1. Introduction

Though it is now clear that accretion of dwarf galaxies likely played a prominent role in creating the Milky Way’s (MW) stellar halo (Searle & Zinn 1978), with strong observational evidence (e.g., Majewski 1993; Majewski, Munn & Hawley 1996; Bell et al. 2008) and a theoretical backing by Λ CDM models (e.g., Bullock & Johnston 2005; Robertson et al. 2005; Abadi et al. 2006; Font et al. 2006a), it is often highlighted that the chemical abundance patterns of current MW satellites are rather different than those of halo field stars, which typically show significantly higher $[\alpha/\text{Fe}]$ than MW dSph stars at the same $[\text{Fe}/\text{H}]$ (e.g., Fulbright 2002; Shetrone et al. 2003; Tolstoy et al. 2003; Venn et al. 2004; Geisler et al. 2005). The reason for these differences remains a matter of speculation. One interpretation is that the dwarf systems that contributed the bulk of the halo were more massive, Magellanic Cloud-sized systems that were accreted and destroyed very early on, so that the chemistry of the accreted stars was necessarily dominated only by enrichment from Type II supernovae (SN II) (Robertson et al. 2005; Font et al. 2006a). Alternatively (or in addition), if current dwarf satellites have experienced both prolonged chemical evolution and tidal disruption, this will naturally lead to evolution in the types of stars that satellites contribute to the Galactic halo (Majewski et al. 2000, 2002).

In principle, one can test the bridge from dwarf galaxy chemistry to halo star chemistry *directly* if one can identify the stars already contributed by the dwarf galaxy to the halo. Perhaps the easiest way to do this is by exploring elemental abundances along the tidal

tails of disrupting dwarf galaxies. Presently, the best known example of a tidally disrupting Milky Way satellite is the Sagittarius (Sgr) dwarf spheroidal (dSph) galaxy, a system that is especially interesting for understanding the issues raised above because the proximity of its core and tails make it particularly accessible to high resolution spectroscopic study, and because the tails produced by its steady assimilation into the MW have been tracked over a substantial length (e.g., Ibata et al. 2001; Majewski et al. 2003, hereafter Paper I; Belokurov et al. 2007) corresponding to several gigayears of tidal disruption (Law et al. 2005, “Paper IV” hereafter). Thus the extensive Sgr tidal stream can provide a key link between dwarf galaxies, tidal disruption and capture, and the chemical evolution and origin of the MW halo.

Exploration of the chemistry of any dwarf galaxy can be used to study star formation environments that are quite distinct from those in the MW, but Sgr provides an interesting case study for chemical evolution in its own right. It is the most luminous and massive of the current MW dSph systems, and has a history punctuated by a number of star formation episodes (Sarajedini & Layden 1995; Layden & Sarajedini 2000; Siegel et al. 2007). This active star formation history quickly elevated Sgr’s mean metallicity to almost solar by about 5 Gyr ago (Bellazzini et al. 2006; Siegel et al. 2007), making it the dSph with the most metal-rich stellar populations known associated with the Milky Way. Because Sgr has been tidally disrupting for at least 2.5-3.0 Gyr (Paper IV), in principle this means that Sgr could have contributed stars with a wide metallicity range to the Galactic halo.

This has been confirmed by the recent analysis of Chou et al. (2007, hereafter Paper V), who measured $[\text{Fe}/\text{H}]$ ranging from -1.4 dex to 0.0 dex for stars identified spatially, dynamically and by spectral type (i.e. the M giants characteristic of the Sgr dSph) with the Sgr stream. Interestingly, the Paper V analysis revealed a strong metallicity gradient along the Sgr stream — proof of a time dependence in the enrichment level of the stars donated to the halo by Sgr, and evidence for preferential tidal stripping of metal poor stars, which has led to divergent metallicity distribution functions (MDFs) between lost and retained Sgr stars. A similar metallicity gradient in the Sgr leading and trailing streams has also been seen by the high resolution analysis of M giants by Monaco et al. (2007). Because stars are typically stripped from the outer parts of dSphs, the changing MDF along the Sgr stream suggests a strong metallicity gradient within the original Sgr system.

Sgr is also chemically interesting because its abundance patterns reveal that while it is undersolar and depleted with respect to the MW pattern for its α -, odd- Z and iron peak-elements among its $[\text{Fe}/\text{H}] \gtrsim -1$ populations, Sgr’s more metal-poor populations seem to have $[\alpha/\text{Fe}]$ that *do* resemble those of the Galactic halo (Smecker-Hane & McWilliam 2002, Bonifacio et al. 2004, Monaco et al. 2005b, Sbordone et al. 2007). Presently these findings

are based on only about 6 Sgr stars having both $[\text{Fe}/\text{H}] < -1$ and measured $[\alpha/\text{Fe}]$ from all of the above studies, as well as a handful of stars from M54 (possibly the nucleus of Sgr — see discussions by Ibata et al. 1994; Sarajedini et al. 1995; Da Costa & Armandroff 1995; Bassino & Muzzio 1995; Layden & Sarajedini 2000; Paper I, but also cf. Monaco et al. 2005a) in the study by Brown et al. (1999). However, if true, the trend may not be unique to Sgr: Abundance patterns (e.g., $[\alpha/\text{Fe}]$) for some of the very most metal-poor stars in other dSphs also seem to overlap those of halo stars of the same metallicity (Shetrone et al. 2003; Geisler et al. 2005; Tolstoy 2005). Thus, if *these* dSph systems experienced tidal disruption, the few very metal poor stars they now hold with MW-like abundance patterns may only represent the residue of a formerly much larger metal-poor population that may have been predominantly stripped from the satellites over their lifetime (see discussion of this in the case of the Carina dSph in Majewski et al. 2002 and Muñoz et al. 2006). Such a scenario could explain the possible origins of the abundance dichotomy between the present dSphs and the Galactic halo.

In this paper we continue our detailed exploration of Sgr stream stars from Paper V with a focus on the chemical trends of the α -element titanium (Ti) and the s-process elements yttrium (Y) and lanthanum (La) along the stream. Our study is based on the largest sample of high resolution spectra yet obtained of Sgr stars, and includes a significant number for stars with $[\text{Fe}/\text{H}] < -0.9$ (§2-3). Collectively, and when combined with additional data from the literature, these stars present a much more complete picture of the chemical abundance patterns for Sgr stars, including the first view of Sgr s-process abundances for $[\text{Fe}/\text{H}] < -0.9$. In §4 we show that, as seen before with smaller samples, the Sgr $[\alpha/\text{Fe}]$ abundances are enhanced and MW-like among the more metal-poor stars, but we also show, for the first time that this trend also arises among the s-process elements we explore. Because of the overall variation of the MDF reported in Paper V, there are increasing numbers of stars with “MW-like” abundances with distance along the stream away from the Sgr core. Thus, the Sgr stream provides a direct connection between the unusual, non-MW-like abundance patterns in the Sgr core and stars with halo-like abundance patterns contributed by Sgr several Gyr ago. In this way, Sgr provides a counter-example of the Robertson et al. (2005) and Font et al. (2006a) hypothesis that the α -enhanced stars of the halo were deposited there long ago.

In §5 we also discuss the implications of the Sgr abundance patterns for the chemical evolution of this dSph. By comparison of the Sgr abundance patterns to those of other MW satellites, we show that Sgr more closely resembles the Large Magellanic Cloud in its chemical evolution than the other dSph-type systems.

Finally, throughout this paper we simultaneously analyze the chemical abundances of a

moving group of M giants among the Sgr leading arm stars at the North Galactic Cap but having different radial velocities than the infalling Sgr leading arm debris there. In Paper V we showed these stars to have a very similar MDF to leading Sgr arm stars stripped several Gyr ago, a result expected if this moving group were constituted by Sgr stars stripped at about the same time. In a demonstration of the technique of “chemical fingerprinting”, we conclude from their peculiar Ti, Y and La patterns, which also match those of the extreme Sgr leading arm, that most of these receding northern hemisphere M giants could represent Sgr *trailing arm* stars in the northern hemisphere.

2. Observations

Our analysis here makes use of the same spectra described in Paper V for six M giant stars in the Sgr core, thirty candidate stars in the Sgr leading arm north of the Galactic plane, ten in the Sgr leading arm but south of the Galactic plane, and thirteen stars in the North Galactic Cap (NGC) moving group, which have velocities much higher and mostly opposite those of the infalling Sgr leading arm there. We selected the first three groups of these stars to be likely members of the Sgr stream not only by their spatial distribution, but also based on their radial velocities, which are appropriate for the Sgr stream at these positions based on Sgr debris models (Paper IV; Figs. 1 and 2 in Paper V). The Sgr core, leading arm north and leading arm south groups represent a dynamical sequence from possibly still bound stars to those stars stripped from Sgr several Gyr ago, respectively. We have argued in Paper V, and will again here (§4), that the NGC moving group stars look to be former Sgr members with chemistry resembling the leading arm south stars; given their positions, velocities and inferred dynamical age, these are most probably Sgr trailing arm stars in the northern hemisphere.

The stars in our sample were observed with the 6.5-m Clay telescope at Las Campanas Observatory and the MIKE spectrograph at $R \sim 19,000$, the 4-m Mayall telescope echelle at $R \sim 35,000$ at Kitt Peak, and the 3.5-m TNG telescope and SARG spectrograph operating at $R \sim 46,000$ in the Canary Islands ¹. The data reduction followed standard procedures and is described in Paper V. Figure 1 shows examples of portions of the spectra from each instrument including the two Ti lines used for our analysis here. Further details of the observations and the positions, photometry and velocities for the program stars can be

¹Based on observations made with the Italian Telescopio Nazionale Galileo (TNG) operated on the island of La Palma by the Fundacion Galileo Galilei of the INAF (Istituto Nazionale di Astrofisica) at the Spanish Observatorio del Roque de los Muchachos of the Instituto de Astrofisica de Canarias.

found in Paper V (with the latter data summarized in Table 1 of that paper).

3. Derivation of Abundances

The required input parameters for the abundance analysis are effective temperature T_{eff} , surface gravity (usually parameterized as $\log g$), and metallicity. The details on the determination of the effective temperature, surface gravity, and iron abundances for our target stars are given in Paper V. The model atmospheres adopted in the analysis were interpolated from Kurucz (1994) grids² and are the same as those used in the analysis in Paper V. Abundances in this study were derived from the LTE code MOOG (Snedden 1973) along with the adopted model atmospheres from Paper V.

We measure the equivalent widths (EWs) of eleven Fe I lines (used to derive the [Fe/H] presented in Paper V), two Ti I lines and one Y II line in a particular part of the spectrum that is relatively free from TiO and other molecular contamination and that was previously investigated by Smith & Lambert (1985; 1986; 1990 — hereafter “S&L”) in their spectroscopic exploration of M giants. These particular elements were chosen not only because they have well-defined, measurable spectral lines, but also because they show distinct abundance ratios (relative to Fe) in many dwarf galaxies when compared to the MW. This circumstance has been found in the core of Sgr itself (Bonifacio et al. 2004; Monaco et al. 2005b; Sbordone et al. 2007), as well as in other dSphs (Shetrone et al. 2003; Geisler et al. 2005) and the Large Magellanic Cloud (LMC; Smith et al. 2002; Johnson et al. 2006; Pompéia et al. 2008; Mucciarelli et al. 2008).

The gf -values for Ti I and Y II were determined by measuring their equivalent widths in the solar flux atlas of Kurucz et al. (1984) and varying the gf -values for each line in order to match the solar titanium and yttrium abundances of $A(\text{Ti})=4.90$ and $A(\text{Y})=2.21$ (Asplund, Grevesse, & Sauval 2005); the adopted solar gf -values are listed in Table 1. The measured EWs of the Ti I and Y II lines for each of our Sgr spectra are given in Table 2. We also include the EW’s measured for several standard stars, which we have analyzed for a comparison and as a control sample.

We analyzed La II via spectral synthesis analysis because this line is affected by hyperfine splitting. An example of the spectral synthesis for this line is shown in Figure 2. The La II line we are interested in is from angular momentum $J = 3$ to $J = 3$, with nuclear spin $I = 7/2$. The lower energy for this transition is 1016.10 cm^{-1} , and the higher energy

²From <http://kurucz.harvard.edu/grids.html>.

is 14375.17 cm^{-1} . There are nineteen hyperfine splitting lines for this transition, and the splitting constants are $A = 3.38$ and $B = 0.84$ for the lower energy level (Lawler et al. 2001). However, the A and B constants for the higher level are unknown. We used various A and B to create a synthetic spectrum and fit it to a very high-resolution Arcturus spectrum. The best-fit A is -30. B is a secondary parameter so it actually doesn't affect the spectrum too much; we have adopted $B = -0.5$ here.

The derived abundance results are summarized in Table 3. For each star, the columns give the derived effective temperature using the Houk et al. (2000) color-temperature relation applied to the 2MASS $(J - K_s)_o$ color, and the derived values of the surface gravity ($\log g$), microturbulence (ξ), abundance $A(X)$, and abundance ratios $[\text{Fe}/\text{H}]$ or $[\text{X}/\text{H}]$ for each element X as well as the standard deviation in the abundance determinations. The details for how we derive the atmospheric parameters (T_{eff} , $\log g$, $[\text{Fe}/\text{H}]$, ξ) can be found in Paper V. The standard deviation represents the line to line scatter (for Ti and Y) and different estimates of the continuum level (for La). We measured two Ti I lines in one order, and two EW measurements of the same Y II line in two adjacent orders. For La II, we have three different abundance measurements from different continuum level adjustments, and give the resulting average La II abundance and standard deviation of those values.

We also have measured abundances for the stars Arcturus, β Peg, β And, ρ Per, and HD 146051, which are nearby K (Arcturus) and M giants that provide a control sample for our abundance work. In Table 4 we summarize literature values (S&L; McWilliam & Rich 1994; Smith et al. 2000) for the atmospheric parameters and abundances for relevant chemical elements of these control sample stars for comparison to our own derived values (no such data are available for HD 146051). Because the references listed adopt somewhat different solar abundances scales, we list the absolute abundances, $A(X)$, rather than abundance ratios in order to facilitate a comparison. We note that S&L used the K giant α Tau as a reference star in their analysis. In order to compute absolute abundances for the control stars we derive abundances for α Tau using the equivalent width measurements in S&L and the model atmospheres and gf values adopted in this study. The derived abundances for α Tau are $A(\text{Fe})=7.52$, $A(\text{Ti})=4.94$ and $A(\text{Y})=2.32$. We used these values and the relative abundance ratios $[\text{X}/\text{H}]$ in S&L to get the absolute abundances of β Peg, β And and ρ Per listed in Table 4. As can be seen, the derived abundances for Arcturus and ρ Per in this work agree with the literature values, within the stated errors and with the standard deviation of the differences less than 0.2 dex. Our derived values of β Peg and β And are lower than those in S&L. This is due largely to differences in the adopted stellar atmosphere parameters.

To explore the sensitivity in the derived abundances to changes in stellar parameters we varied T_{eff} , $\log g$ and microturbulence for the control stars and tabulate the abundance

changes in Table 5. This table shows the sensitivities of the Fe I, Ti I, Y II and La II lines corresponding to changes in T_{eff} by +100 K, $\log g$ by +0.2 dex (where g is measured in cm s^{-2}), and ξ by +0.2 km s^{-1} , respectively.

With these dependencies in hand, we derive the abundances for the M giant comparison stars adopting the previously published stellar parameters from S&L. The resulting abundances are provided as separate entries in Table 4, and indicate general agreement, within calculated uncertainties, for $A(\text{Fe})$ values when similar atmospheric values are adopted for the M giant comparison stars. This exercise also demonstrates how the derived $A(\text{Y})$ values much more closely match the previously derived values for these stars when we adopt similar stellar parameters. The lower $A(\text{Y})$ we find in this paper for the control stars arises primarily from our derivation of lower $\log g$ for these stars. As previously mentioned in Paper V, the S&L studies predated the availability of Hipparcos parallaxes, and therefore they adopted higher $\log g$ values from less accurate absolute magnitudes.

Finally, our analysis shows that, in general, we tend to find $A(\text{Ti})$ slightly lower by about 0.2-0.3 dex compared to S&L, even when similar atmospheric parameters are adopted for the M giants. Note however that different sets of Ti lines have been used in the two studies and that different families of model atmospheres can also account for some of the abundance differences. In addition, when comparing the derived abundances with the previously published results from S&L one has to keep in mind that S&L computed only relative abundances using α Tau as a reference star with the underlying assumption that its abundance distribution is approximately solar. Indeed, Kovács (1983) conducted a detailed absolute abundance analysis for α Tau and validated this assumption at a level of roughly ± 0.2 dex. Absolute abundances computed from the relative abundances published in S&L will carry the uncertainty in the underlying α Tau abundance distribution.

Further circumstantial evidence that our Ti abundances are more reliable comes from a comparison of our derived $[\text{Ti}/\text{Fe}]$ for the control stars to the $[\text{Ti}/\text{Fe}]$ trend of other disk stars, as shown in the top panel of Figure 3 (where the control sample stars are shown as brown stars); as may be seen, were we to shift our Ti abundances several 0.1 dex higher to make them more consistent with the S&L values, all five of the control stars (including HD146051 now) would have $[\text{Ti}/\text{Fe}]$ above the mean for disk stars of similar $[\text{Fe}/\text{H}]$, and in some cases anomalously so. In addition, as we will show in Figures 3 and 10 below, a several tenths of a dex offset in $A(\text{Ti})$ would make the already high $[\text{Ti}/\text{Fe}]$ abundances found for metal poor Sgr stars compared to other dSphs and the LMC even more extreme.

4. Derived Abundance Patterns

and Variation Along the Sgr Stream

4.1. Abundance Differences Compared to Milky Way Field Stars

To verify whether our sample is indeed dominated by members of the Sgr stream, rather than random MW field stars, we appeal to the well-known abundance pattern differences between the MW and dSph satellites in general, and between the MW and the Sgr dSph in particular. In principle, one might expect that stars recently stripped from dSph systems to bear similar peculiar chemical hallmarks as the stars they left behind in the dSph core. The promise of “chemical fingerprinting” stars to their birth systems has long been discussed (Freeman & Bland-Hawthorne 2002; De Silva et al. 2007), but has yet to be used much in practice. A side benefit of our study is that it lends itself to a direct test of the viability of chemical fingerprinting in a well-defined, fairly controlled context (i.e., testing a sample of stars specifically selected to have been born in one particular system – Sgr — against contamination from stars from another system — the MW). In addition, in §4.2 we *apply* chemical fingerprinting to test the notion that the NGC group of stars may be from Sgr.

It has long been observed that present dSph stars are typically underabundant in $[\alpha/\text{Fe}]$ compared to Milky Way stars at the same $[\text{Fe}/\text{H}]$, presumably a result of the much slower enrichment history of these smaller systems, which allows the products of Type Ia supernovae (SN Ia) (including much of the iron) to be introduced at lower overall metallicities. The same underabundance trend is found for various light s-process elements, like yttrium, which are thought to be converted to heavier s-process elements (like lanthanum) by high neutron exposure in low mass asymptotic giant branch (AGB) stars; thus, low Y and high La abundances are also an indication of a slow enrichment star formation history, at least compared to the Milky Way.

Detailed abundance studies of the Sgr core have shown similar overall trends in abundances patterns as other dSphs, but also some trends apparently characteristic of the Sgr system itself. For example, Smecker-Hane & McWilliam (2002) and McWilliam & Smecker-Hane (2005) found that high metallicity ($[\text{Fe}/\text{H}] > -1$) Sgr stars show extraordinarily enhanced heavy s-process (e.g., La) abundances, while at the same time these stars have low abundances of Mn and Cu. Similar chemical trends are also found in the LMC (Johnson et al. 2006; Pompéia et al. 2008). Since manganese and copper yields from SN II decrease, relative to iron, in lower metallicity supernovae, the low values of $[\text{Mn}/\text{Fe}]$ and $[\text{Cu}/\text{Fe}]$ could be the result of nucleosynthesis from low-metallicity SN II, while the large values of $[\text{La}/\text{Fe}]$ are the product of the s-process yields from low-metallicity, low-mass AGB stars. These patterns can arise from intense star-formation bursts, along with loss of some SN II ejecta via galactic winds, followed by long quiescent periods in the dSph. After long periods of time (several

Gyr), low-mass, low-metallicity AGB stars eventually add significant amounts of ejecta into the interstellar medium (ISM) and leave their signature on the highest metallicity stars.

Figures 3-6 show the distributions of $[\text{Ti}/\text{Fe}]$, $[\text{Y}/\text{Fe}]$, $[\text{La}/\text{Fe}]$, and $[\text{La}/\text{Y}]$ as a function of $[\text{Fe}/\text{H}]$ for all of our targeted stars (middle panels), for those of MW and other dSph stars (top panels), and for our targeted stars superposed on those of LMC stars (bottom panels). The MW abundance distributions have been taken from Gratton & Sneden (1994), Fulbright (2000), Johnson (2002) and Reddy et al. (2003). The other dSph data are from Shetrone et al. (2001; 2003), Sadakane et al. (2004) and Geisler et al. (2005). The LMC data are from Johnson et al. (2006), Pompéia et al. (2008) and Mucciarelli et al. (2008).

It is immediately obvious from inspection of Figures 3-6 that the bulk of our sample stars do not share the same chemical abundance patterns as Milky Way stars. To quantify this assessment, we fit linear trends to the Milky Way distributions (the lines shown in Figs. 3-6), and determine the dispersions around those trends for Galactic stars: 0.15 dex for $[\text{Y}/\text{Fe}]$ and 0.12 dex for $[\text{La}/\text{Fe}]$. For the $[\text{Ti}/\text{Fe}]$ versus $[\text{Fe}/\text{H}]$ distribution we fit two linear trends on either side of the apparent Milky Way transition at $[\text{Fe}/\text{H}]=-0.7$, and find dispersions of 0.10 and 0.05 dex to either side of that break, respectively. (These measured dispersions represent both the intrinsic dispersion of abundances as well as measurement errors from the various surveys of MW stars.) For each of our M giants we determine the number of standard deviations, N_σ , away from the Milky Way mean trend that star is at its $[\text{Fe}/\text{H}]$ in each of the distributions shown ($[\text{Ti}/\text{Fe}]$, $[\text{Y}/\text{Fe}]$ and $[\text{La}/\text{Fe}]$ as a function of $[\text{Fe}/\text{H}]$, Fig. 7). These deviation measures are tabulated in columns 2-4 of Table 6. We also derive an average deviation for all three trends (column 6 of Table 6). These deviations allow us to characterize how “Milky Way-like” each star is; we adopt as a definition of “Milky Way-like” those stars that always lie within 1.5σ of the mean MW abundance trends. By this definition, only four stars from the 30 leading arm north sample, no stars in the leading arm south sample, and one star from the 13 NGC sample have abundance patterns approximating “MW-like”; these stars are designated with overlying “cross” symbols in Figure 7 (as well as in Figure 9, described below). For comparison, by our adopted definition of “MW-like” we would also classify four of 27 of the bona fide Sgr stars from Monaco et al. and Sbordone et al. as “MW-like”. This simple analysis attests to the true peculiarity of the stars in our sample by a Galactic standard, and that there is likely little contamination by MW stars.

Note that in Paper V we had divided the Sgr leading arm north group into a “best” (the fainter and farther stars that are most likely to be in the Sgr leading arm) and a “less certain” subsample. The latter included stars with brighter magnitudes ($K_{s,0} < 7.5$) that we considered the most susceptible to contamination by Galactic (thick disk) stars as well as those stars closest to the Galactic bulge. We showed in Paper V (see, e.g., Fig. 9

of that paper) that the metallicity distributions of the “best” and “less certain” samples were similar in shape, spread and mean values. Further analysis of the relative abundance patterns between these two subsamples here also reveals no obvious distinctions: Figure 8 shows that there is no apparent difference in the overall chemical patterns between the less certain and best LN subsamples, even though the latter are at projected distances more commensurate with those predicted by the Paper IV model for the Sgr leading arm in the Northern Hemisphere and observed for other proposed Sgr leading arm tracers (e.g., the K/M giants and blue horizontal-branch stars (BHBs) from SDSS/SEGUE spectra by Yanny et al. 2009, and the RR Lyrae stars (RRLs) with large negative Galactic Standard of Rest velocities (v_{GSR}) in the Virgo stellar stream (VSS) region likely to be Sgr stars by Prior et al. 2009b). Therefore, we continue to see no evidence that the two LN subsamples are stars of a different origin and, given the other evidence presented here that they are all most likely to be Sgr stream stars, we continue to consider them together as the single “Sgr leading arm north sample” in this paper.³

Figure 9, which shows the distribution of $[Y/Fe]$ versus $[Ti/Fe]$, further demonstrates the true distinction between our sample stars and those in the standard Galactic populations; stars in our Sgr sample are shown color-coded by their Sgr system grouping in the top panel. We also compare the MW stars with those of other dSph and LMC stars on the middle and bottom panels, respectively. Figure 9 shows a striking segregation of stars by their parent system (particularly by $[Y/Fe]$), and one that further illustrates the differences in chemical evolution between stars we have selected to be Sgr-members and the nominal MW populations (see §5). In the top panel of Figure 9 we have marked with large crosses those stars that were deemed most MW-like by the above σ analysis; as might be expected, these tend to lie closest to the V-shaped distribution of MW stars, but even then not in the main locus of MW stars, but, rather, skirting it. Figure 9 further reinforces the conclusion that the sample of M giants we have observed should have very little contamination by nominal MW field stars, and this includes stars we have selected to lie in the NGC group (see §4-2). Furthermore, we notice that stars from the other dSphs as well as the LMC sit in the bottom

³It is perhaps worth mentioning that present Sgr stream models, such as that presented in Paper IV, show that the leading arm may wrap a second time around the Galactic center — and with the debris in the second leading arm wrap lying closer to the Sun in the Northern Hemisphere than the debris in the first wrap. This is a potential source of contamination of the LN sample by further extensions of itself; however, if the trend between the LN and LS stars is extrapolated, stars in a second leading arm debris wrap should be even more metal-poor on average than the LS sample. That there is no clear distinction in metallicities between the closer and farther LN stars — while the LS stars *are* more metal poor on average — suggests that this “self-contamination” of the LN sample by debris from the second wrap of the Sgr leading arm may not be significant.

left part of Figure 9 (middle and bottom panels), so that they share a similar — but not exactly the same — distribution as our Sgr stars. It is worth noting that about a third of the stars selected to be from the Sgr system (including one or two Sgr core stars) have higher $[\text{Ti}/\text{Fe}]$ than the bulk of the dSph and LMC stars (a feature seen also in Fig. 3). Nevertheless, since about 2/3 of the “Sgr system” stars do share the same chemical patterns as other dwarf galaxy systems in Figure 9, we can not rule out the possibility that a small number of these particular Sgr stars are from other dwarf satellite debris. We discuss this point further in §4.3.

The observed deviation of our selected Sgr stream stars away from MW abundance trends as a function of $[\text{Fe}/\text{H}]$ is illuminating. Deviation trends can be used as a quantitative chemical marker, and combinations of abundance patterns for different elements are thought to provide unique, or at least fairly distinctive, chemical fingerprints that can be used to identify the star formation sites (e.g., the parent galaxies) of specific stars. For example, inspection of the $[\text{Ti}/\text{Fe}]$ vs $[\text{Fe}/\text{H}]$ trends shown in Figure 3 (top and middle panels) and Figure 7 reveal clear differences between our sample of likely Sgr stars and MW stars: While there is a general agreement in the $[\text{Ti}/\text{Fe}]$ levels for the MW and Sgr stars at the lowest metallicities ($[\text{Fe}/\text{H}] \lesssim -1.0$) — where both the Sgr and MW stars are equally enhanced in $[\alpha/\text{Fe}]$, a feature that betrays the signature of prevalent SN II enrichment — the differences in abundance trends increase rapidly above $[\text{Fe}/\text{H}] \sim -1.0$, with the great majority of Sgr stream stars falling below the MW trend. The latter trend reflects the lower star formation efficiency and/or slower chemical enrichment (and, thus, greater relative SN Ia yields) of Sgr stars relative to those of the MW (see §5).

Meanwhile, the trend for $[\text{Y}/\text{Fe}]$ shows the Sgr stars to be underabundant with respect to the MW and subsolar over the whole range of sampled $[\text{Fe}/\text{H}]$ (Figs. 4 and 7). On the other hand, $[\text{La}/\text{Fe}]$ is primarily below the MW trend until $[\text{Fe}/\text{H}] \sim -0.5$, when it quickly rises well above the MW level. This trend was previously found by Smecker-Hane & McWilliam (2002). The relative abundances of heavy to light s-process elements shown by $[\text{La}/\text{Y}]$ (Fig. 6) accentuate the differences between Sgr and MW stars at all metallicities. We further interpret the meaning of these various trends in §5.

4.2. Chemical Trends Along the Sgr Stream and Chemical Fingerprinting of the North Galactic Cap Stellar Group

Presently, the only known dSph satellite of the MW known to contain a significant population of M giants is the Sgr system. While the Magellanic Clouds contain large numbers

of M giants, the analyses undertaken in Paper I and elsewhere have revealed no evidence of any M giant tidal structures from either of the Magellanic Clouds. At low Galactic latitudes M giants are found associated with the Monoceros/Galactic Anticenter Stellar Structure (GASS, Rocha-Pinto et al. 2003), but it is still not clear whether this structure is a tidal stream or a part of the MW disk (e.g., Martin et al. 2004b; Momany et al. 2004, 2006; López-Corredoira et al. 2007). The only other MW substructure that is certainly a tidal debris remnant and known to contain M giant stars is the more distant, Triangulum-Andromeda (TriAnd) star cloud (Rocha-Pinto et al. 2004), also at low Galactic latitudes ($-40^\circ < b < -20^\circ$). For higher Galactic latitudes, the analysis of M giant distributions in Paper I showed that a major fraction ($\gtrsim 75\%$) of M giants found in the halo away from the Galactic plane lie along the Sgr orbital plane; since overall the presence of M giants in other MW dSphs or substructures is relatively rare, the concentration of high latitude Galactic M giants along the Sgr plane suggests that the vast majority of these stars were indeed contributed by the Sgr dSph.

This proposition received further support with subsequent study of the radial velocities of these M giants, which show most of them also to lie in correlated trends of velocity with Sgr orbital plane longitude (Majewski et al. 2004, “Paper II” hereafter; Paper IV) corresponding to the Doppler motion of the most recently stripped (e.g., within the last 1-2 Gyr) Sgr debris as it wraps around the Galactic center (see Paper IV). Recently, Yanny et al. (2009) have shown that our adopted radial velocity (RV) sequence for Sgr stars in the northern sky (e.g., as shown in Figure 2 of Paper V) is well matched by SDSS/SEGUE-derived radial velocities for candidate Sgr K/M giants and blue horizontal-branch stars (BHBs) along the leading arm. This correspondence lends further credence to the notion that most of our RV-selected Sgr leading arm stars are indeed from the Sgr dSph.

However, not *all* M giants in the Sgr plane are found to lie along the primary velocity trends of this most recently lost debris. In particular, a number of radial velocity “outliers” have been found in the southern Galactic hemisphere, mostly in the Sgr longitudinal range $\Lambda_\odot = 20 - 90^\circ$ (Paper II). These particular stars have been associated with older parts of the Sgr leading arm that have already passed below the Galactic plane and that form a new loop around the Galactic plane (Paper IV); a fraction of these stars constitute our “Leading Arm South (LS)” sample in Paper V, where we show them to have a more metal-poor distribution overall than the dynamically younger, “Leading Arm North (LN)” sample. Figures 3-7 in this paper show these LS stars to also have abundance patterns indicating that they are not only dynamically older Sgr stream stars (i.e. stripped from Sgr longer ago), but also likely to have actually formed earlier than the LN stars on average. Specifically, the LS stars show a higher mean [Ti/Fe] level (0.26 dex) than that of either the Sgr core (-0.05 dex) or LN (0.13 dex) samples, which demonstrates that, on average, the LS stars were formed when

enrichment in Sgr was still dominated by SN II. This difference in $[\text{Ti}/\text{Fe}]$ trends between the LS and LN is consistent with the age-metallicity relation of Sgr (Siegel et al. 2007), which shows that stars of the mean metallicity of the LS ($[\text{Fe}/\text{H}] = -1.1$) were formed on average ~ 11 Gyr ago, only ~ 1 -2 Gyr after the oldest known populations in Sgr and before significant numbers of SN Ia progenitors (mass transfer binaries) from those earliest populations could have evolved to supernova stage and introduced significant iron yields into the Sgr ISM. On the other hand, Siegel et al.’s age-metallicity relation suggests that stars of the mean metallicity of the LN, $[\text{Fe}/\text{H}] \sim -0.7$, were formed about 7.5 Gyr ago, or well after the onset of routine SN Ia enrichment. As pointed out in Paper V, that the dynamical age difference between the LN and LS stars is only about 0.8 Gyr whereas the mean metallicity difference between these samples is $\Delta[\text{Fe}/\text{H}] \sim -0.4$ dex (and that both of these differ significantly in mean metallicity from that of the core stars, at $\langle [\text{Fe}/\text{H}] \rangle = -0.4$) suggests that the Sgr progenitor must have had a significant radial metallicity gradient before disruption. The age-metallicity relation of Siegel et al. implies that there must have been a significant mean age gradient as well.

A second group of M giant stars that do not lie along the primary velocity sequences of more recently stripped Sgr stream stars are those we have called the North Galactic Cap (NGC) group, which have velocities more positive than the LN stars in the same part of the sky (Paper II). In Paper V we showed that our sample of these stars has a similar metallicity distribution to that of the LS sample, and, by reference to the Paper IV model, we concluded by their position, velocity and metallicity distribution that the NGC group might be the trailing arm counterpart above the Galactic plane to the Leading Arm South group below the Galactic plane — that is, the two groups are Sgr debris of the same dynamical age. Figures 3-6 and Figure 9 further support this notion by showing that the abundance patterns of the NGC group very closely align with those of the LS. Not only does this comparison chemically fingerprint the NGC stars as likely Sgr debris, but it places these stars into the Sgr disruption dynamical time sequence, and in a place in that sequence that makes sense within the context of the Paper IV model for trailing arm debris in the North Galactic Hemisphere that was stripped at the same time as the LS stars, i.e. roughly 3 Gyr ago (see green debris in Fig. 1 of Paper IV or Fig. 1 of Paper V). By tagging the NGC group of stars to the Sgr trailing arm through its abundance patterns we demonstrate here one of the earliest direct applications of the concept of “chemical fingerprinting”.

4.3. Caveats and Alternative Scenarios

Despite the above conclusions regarding the association of all four of our target subsamples to the Sgr system, the recent discovery of the “Virgo stellar stream” (VSS, Duffau et al. 2006; Vivas et al. 2008) and “Virgo overdensity” (VOD, Jurić et al. 2008) shows these features to span a wide range of Northern Galactic Hemisphere sky (over 1000 deg² in the case of the VOD; Jurić et al. 2008), and it is worth evaluating whether any of our subsamples — namely the Sgr LN stars and the NGC groups, which are also in the Northern Galactic Hemisphere — could be related to these extensive Virgo structures. Both the VSS and VOD have been explained in terms of debris from dSph mergers with the MW, so could account for high northern latitude stars with non-MW-like abundance patterns. We compare five properties of the LN and NGC groups against those of the VSS and VOD to demonstrate that there is unlikely a connection between the latter two halo substructures and the LN and NGC group stars.

(1) *Distances:* The distance of the VSS is ~ 19 kpc (Duffau et al. 2006; Newberg et al. 2007; Prior et al. 2009), while the VOD is estimated to have a distance of ~ 6 -20 kpc (Jurić et al. 2008; Vivas et al. 2008; Keller et al. 2009). Using the [Fe/H] values measured for the M giants in Paper V, we have used the corresponding isochrones from Marigo et al. (2008) and the observed, dereddened K_s magnitudes to estimate photometric parallax distances to each of our stars. This exercise is one fraught with large uncertainties, since for each star we have to assume an age (which can be roughly deduced from the age-metallicity relation, e.g., that in Siegel et al. 2007), a mean $[\alpha/\text{Fe}]$ (which may or may not be well traced by [Ti/Fe]), and whether a particular star is on the first or second ascent giant branches; nevertheless we attempted the exercise to get a rough idea of whether the stars could be at the distances of the VSS or VOD.

Based on the rough photometric parallaxes we find that all of the LN and NGC stars are closer than the VSS, whereas a large number of the LN and NGC stars are in the range of distance quoted above for the VOD. Fortunately, other properties of these stellar systems give more definitive discrimination between them (see below).

(2) *Sky Positions:* The VSS is a narrow structure currently mapped from $l = 279^\circ$ to 317° and $b = 60^\circ$ to 63° (Duffau et al. 2006); even extrapolating that swath along the same great circle, the VSS hardly intersects the region of the sky covered by the NGC group sample, which, in any case, is much more broadly dispersed than the relatively narrowly confined, $\sim 3^\circ$ -wide VSS. The positions of only two LN stars overlap the extrapolated swath of the VSS, but the velocities of these two stars (stars 1236549–002941 and 1319368–000817) grossly mismatch that expected for the VSS at their positions.

On the other hand, the VOD *is* much more broadly distributed on the sky, covering around 1000 deg² with a center at $(l, b) \sim (300^\circ, 65^\circ)$; however, the area of the sky covered by this excess (Jurić et al. 2008) is very different than the areas covered by either the LN or NGC samples. Only a mere seven stars from the LN and one star from the NGC group subsamples even lie in the most liberal definition of the angular extent of the VOD.

(3) *Velocities*: A number of VSS stars have had spectra taken that show them to have v_{GSR} spanning $\sim 100 - 130 \text{ km s}^{-1}$ (Duffau et al. 2006; Newberg et al. 2007; Prior et al. 2009). The only available velocity information on the VOD comes from the QUEST RR Lyrae star survey (Vivas et al. 2008) combined with a sample of BHBs from the SDSS survey (Sirko et al. 2004). Vivas et al. find that there are three moving groups in the VOD region, with average $v_{GSR} = +215, -49$ and -171 km s^{-1} , respectively. These authors suggest that the VOD actually consists of the VSS plus other halo substructures. The stated v_{GSR} range of the VSS has the opposite sign as most of the Sgr LN stars, but does cross the range of v_{GSR} spanned by our NGC group M giants. However, no more than three of our NGC sample stars, and five of the LN sample stars barely match *both* the position and velocity distribution of either the VSS or VOD.

(4) *Metallicities*: The M giants in our Sgr sample stretch broadly from solar metallicity down to the the lowest metallicity where M spectral type giants can form ($[\text{Fe}/\text{H}] \sim -1.4$), but there is no correspondingly high metallicity population that has been identified with the VSS and VOD thus far. The metallicity of VSS RR Lyrae stars is ~ -1.86 to -1.95 (Duffau et al. 2006; Prior et al. 2009), and VOD main sequence stars are at ~ -2.0 (An et al. 2009). Since the metallicity of RR Lyraes can extend to solar metallicity (as seen, for example, in the local MW disk; Layden 1994), the lack of metal-rich RRLSs found in the VOS or VVS suggests that the stellar populations in the VSS/VOD are metal-poor in the whole, and even slightly more metal-poor than the RR Lyrae stars found among the Sgr tidal debris (which have $[\text{Fe}/\text{H}] \sim -1.7$ to -1.8 ; Vivas et al. 2005, Prior et al. 2009b, Starkeburg et al. 2009).

(5) *Evidence for M giant populations*: Of course, the very existence of M giants in a stellar population is determined by its metallicity, with only relatively metal-rich populations making first ascent giant branch stars that late in spectral type. There is no evidence for M giant stars distributed kinematically and positionally as counterparts to the other VSS/VOD tracers. If either the VSS or VOD structures contained an M giant population, one might expect at least a concentration of those M giants at the densest, “core” parts of those structures as traced by other stellar types; yet the analysis of 2MASS M giants in Paper I, as well as more recently by Sharma et al. (2009, in prep.), reveals no concentration of M giants either centered on the VOD or following the VSS. On the other hand, that the Sgr stream *does* contain M giants, that the M giants in the Galactic halo are almost entirely concentrated

along the Sgr orbital plane (except at the very lowest latitudes, where Monoceros/GASS and TriAnd contribute), and that the M giants we have selected are generally matched in position on the sky with known Sgr features makes it far more likely that the LN and NGC group stars are associated with Sgr than the VSS or VOD.

On the other hand, there does remain an alternative scenario to that we have adopted as most likely here (namely that all of our subsamples are related to the Sgr system) that is presently very difficult to discriminate against. It has recently been proposed that all or some satellites of the MW may have been accreted as one or more groups of galaxies (Li & Helmi 2008; D’Onghia & Lake 2008; Metz et al. 2009). For example, D’Onghia & Lake (2008) proposed that an “LMC group” — composed of the LMC, Small Magellanic Cloud (SMC), Sgr and other satellite galaxies — were originally part of a collection of galaxies once bound to each other and that later fell into the MW together. This hypothesis can explain the planar orbital configuration of some dSphs in the MW halo (e.g., Kunkel 1979; Lyden-Bell 1982; Majewski 1994; Palma et al. 2002; Metz et al. 2008), and could explain the planar configurations of tidal debris, even if that debris ultimately derived from different satellites. With slight differences in initial orbits of the parent dwarf galaxies, that debris today might have differing orientations and velocities, despite being in nearly the same plane and having the same general direction of angular momentum; in principle, therefore, one could explain our various M giant samples lying in a largely planar distribution as deriving from different parent accreted dwarf galaxies, but perhaps parents that fell into the MW together.

One motivation for proposing such an “infalling group” scenario in the specific case of the Sgr system is that it might provide an origin for the recently discovered, but not yet definitively-explained bifurcation of the northern Sgr stream leading arm as seen in the SDSS imaging (Belokurov et al. 2006; Fellhauer et al. 2006).⁴ On the other hand, Yanny et al. (2009) find not only the metallicities, but the velocities and distances to be indistinguishable in the two pieces of the bifurcated SDSS Sgr feature. This suggests a strong coherence in star formation and chemical enrichment histories, at least for those stars along the bifurcated, Northern Hemisphere Sgr arm — and, were such a coherence between two parent systems to exist, it would be very hard at present to distinguish this from a single parent origin (i.e. the known Sgr core) for all of the debris. At present, in the absence of evidence supporting

⁴We point out that Fellhauer et al. (2006) attribute one each of the two Sgr structures in the SDSS Northern Galactic Hemisphere data to the leading and trailing arms of the Sgr stream, respectively. But this explanation is not consistent with the predictions of the distances of these structures by the Paper IV model, which was designed to constrain not only the positions of Sgr data on the sky (the main criteria used by the Fellhauer et al. 2006 Sgr model), but the extant Sgr stream velocity data as well. Furthermore, Yanny et al. (2009) suggest that the two branches might be from debris that was stripped at similar times, due to the similar velocities, metallicities, and relative densities of K/M giant, BHB, and F-turnoff stars.

multiple parent systems producing multiple M giant substructures along the same plane in the sky, we prefer the most straightforward interpretation for the connection of the LN and LS groups as parts of a single Sgr leading arm, as well as the identification of the NGC group with (a diffuse distribution of) the Sgr trailing arm.

In conclusion, detailed chemical abundance analysis of our various samples demonstrates that these stars are by and large dSph-like and with little contamination by the nominal Milky Way populations, halo or disk. Because the leading arm stars were also pre-selected to be in the Sgr stream and to follow the expected velocity trends for Sgr debris, because they form a clear and logical chemical sequence, and because no evidence for other M giant tidal debris from any other satellite is found to intersect the Sgr stream in relevant parts of the sky, and, furthermore, because all evidence continues to support that the bulk of all high latitude M giants have been contributed from the Sgr system, we conclude that the vast majority of our leading arm stars must be from the Sgr dSph. Since the NGC sample stars share similar chemical patterns of Sgr LS stars, we conclude that they are likely Sgr stars as well, but this hypothesis requires them to be from the trailing arm debris due to their peculiar velocities. Therefore, we propose that all of our M giant samples, taken as a group, together paint a chemical portrait of the Sgr dwarf as it appeared ~ 3 Gyr ago.

Finally, we close this discussion of caveats with a warning to the reader that although we believe the LN, LS and even the NGC group stars to be primarily constituted by stars stripped from the Sgr dSph system, these samples represent highly biased sets of such stars by distance: In the present high resolution spectroscopic study we selected targets that we expected to be Sgr stream members but that were also bright enough to allow echelle spectroscopy to adequate S/N for chemical abundance analysis. Moreover, we selected the target stars for this study (and that in Paper V) from an input catalog — those M giants that had radial velocities from medium resolution spectroscopy (e.g., Paper II, Paper IV) — that itself shares some degree of the same bias. Given this strong prejudice for the closest, brightest Sgr members we could find, one should exercise due caution in how these stars are used. For example, one should not use the stars in Table 3 to constrain the mean distances of different parts of the Sgr stream since those mean distances no doubt lie beyond the stars presented here; the latter are likely several or more σ outliers in the distance distribution of Sgr stream stars.

5. Global Chemical Evolution of the Sgr System

We can take advantage of our entire Sgr high resolution core + tidal tail sample to build the most complete (in terms of metallicity span) chemical portrait of the Sgr progenitor yet

assembled; this portrait is summarized by the middle panels of Figures 3-6 as well as Figure 9. Chemical evolution is driven by the cycle of nucleosynthesis and subsequent transfer of nucleosynthetic products into the environment for incorporation into future generations of stars. Chemical evolution models guide the interpretation of observed patterns in a galactic system such as those demonstrated in Figures 3-6 and 9.

5.1. [Ti/Fe]

For example, as mentioned above, α elements are mainly produced by SN II while iron is synthesized largely by SN Ia, whose progenitors have a lifetime of ~ 1 Gyr. Therefore, $[\alpha/\text{Fe}]$ is high for early chemical enrichment in a stellar system and then declines as SN Ia “turn-on”. Titanium acts mainly as an α element, and from its trend with $[\text{Fe}/\text{H}]$ we can infer how far chemical evolution proceeded in the first ~ 1 Gyr of the system’s life, an indication of the initial star formation rate (SFR). Figure 3 shows that the downturn in $[\text{Ti}/\text{Fe}]$ happens at around $[\text{Fe}/\text{H}] = -0.9$ for Sgr, which is only a few tenths of a dex lower than the transition seen in the MW field star population; this suggests a lower early SFR in Sgr than for the MW field population (Monaco et al. 2005b; Sbordone et al. 2007). Alternatively, Lanfranchi et al. (2006) argue that initially Sgr may have started out with a high star formation efficiency — at least higher than that of other dSphs — but the resulting intense galactic wind acted to substantially squelch the SFR. Lanfranchi et al. claim that most of the observed Sgr stars formed after the beginning of the wind, which explains why they have lower $[\alpha/\text{Fe}]$ than MW stars.

Figure 3 also shows the $[\text{Ti}/\text{Fe}]$ trends for the LMC and other dSphs, which are very different from the trends for the MW and the metal-poor Sgr stars. The chemical differences among these various systems are due to their unique star formation histories (Venn et al. 2004; Johnson et al. 2006). As may be seen, in the LMC and other dSphs, the $[\text{Ti}/\text{Fe}]$ is low over all $[\text{Fe}/\text{H}]$ probed, due to a lower early SFR, which is the result of low star formation efficiencies and high galactic winds (Geisler et al. 2007), and also probably because of fewer high-mass SN II in these small systems (Woosley & Weaver 1995; Tolstoy et al. 2003; Pompéia et al. 2008).

We also find the metal-poor Sgr stars (with $[\text{Fe}/\text{H}] \lesssim -1.2$) to have high Ti abundances, similar to the trend for the MW. This implies that the early chemical composition of Sgr was more like the MW (Shetrone 2004) than the LMC and other dSphs; from a similar comparison of $[\alpha/\text{Fe}]$ abundances of low $[\text{Fe}/\text{H}]$, Monaco et al. (2005b) conclude that the Sgr progenitor was probably a relatively large, star forming, gas-rich object. On the other hand, Monaco et al. (2005b) also suggest Sgr should have had a different subsequent chemical

evolution from the MW and other Local Group galaxies due to the strong and disruptive dynamical interactions this system has clearly had with the MW; these interactions in a gas-rich system can typically trigger star formation activity (e.g., Kravtsov et al. 2004; Zaritsky & Harris 2004).

5.2. s-process Elements

The s-process elements are thought primarily to occur during thermal pulses in the intershell convection zone in low mass AGB stars. The neutron flux per seed nucleus is roughly inversely proportional to the metallicity of the AGB. Therefore, at low metallicities AGB stars produce heavier s-process elements like La more efficiently than lighter species like Y, all of the way up to the formation of the heaviest s-process element, Pb, in the most metal-poor environments (see the review by Busso et al. 1999 and 2004). Figures 5-6 show upturns in [La/Fe] and [La/Y] for Sgr at [Fe/H] ~ -0.5 . Since [La/Y] is enhanced in metal-rich Sgr stars, the high ratio of heavy to light s-process elements ([hs/ls]) among the metal-rich stars indicates a strong contribution from low-metallicity AGB progenitors (Smecker-Hane & McWilliam 2002), and a slower SFR of Sgr than the MW, so that the low-metallicity AGB yields have enough time to contaminate the ISM (Venn et al. 2004; Pompéia et al. 2008). On the other hand, Sgr and LMC stars at lower metallicity show similar trends to MW stars, particularly in Y and La; this indicates that these stars might be among the first ones formed because they were not yet contaminated by the AGB yields (Johnson et al. 2006; Mucciarelli et al. 2008). Moreover, models for the evolution of old, gas-poor dSphs (e.g., Sculptor) predict subsolar Y over all [Fe/H] probed, and an upturn in La abundance at [Fe/H] ~ -1.6 , due to the appearance of the products of metal-poor AGB progenitors in the ISM (Fenner et al. 2006; Gibson 2007). The patterns of La in Sgr basically agree with the prediction of the gas-poor dSphs, except the upturn in Sgr occurs at higher [Fe/H]. That suggests a higher early SFR of Sgr than other dSphs, and the high [hs/ls] can be seen as another “clock” of star formation, in addition to the $[\alpha/\text{Fe}]$ ratio.

5.3. Relative Galaxy Star Formation Rates

Figures 3-6 have demonstrated abundance trends for Sgr that distinguish it from the MW and other MW satellites. Several of these differences relate to the onset of specific chemical chronometers, such as the contribution to the gaseous environment of the yields from SN Ia (seen as a decrease in [Ti/Fe]) and metal-poor AGB (seen as an increase in [La/Y], for example), where the [Fe/H] corresponding to the chemical signature is correlated to the

SFR prior to the creation of that signature. A comparison of the above two chronometers ([Ti/Fe] and [La/Y]) suggests a natural sequence in relative SFRs from the other MW dSph systems (lowest SFRs), to the LMC (a modest SFR), and Sgr (the highest SFR among the MW satellites), based solely on the positions of the transitions in chemical properties in [Fe/H].

To emphasize the point that the chemical histories of the MW satellites likely differ primarily as a function of their SFRs, we modify the comparisons of the chemical properties of Sgr to those of the LMC and other dSphs as shown in Figures 3-6 by shifting the distributions of the dSph ensemble and the LMC by $\Delta[\text{Fe}/\text{H}] = +1$ and $+0.4$, respectively (these particular values were selected by eye for illustrative purposes only). The results, shown in Figure 10, reveal a much closer agreement in the overall shapes of the abundance trends shown, suggesting even the possibility of a “universal” chemical enrichment pattern among MW satellites, with the primary difference being the [Fe/H] placement of the pattern, which itself is a function of the early SFR.

It is immediately obvious from Figures 3-6 and Figure 10 that Sgr much more closely matches the overall chemical evolution of the LMC than it does other MW dSphs. Indeed, their similar chemistries suggest that it may be reasonable to consider the LMC — a late type, dwarf spiral or irregular galaxy — as a more appropriate paradigm for the pre-interaction state of Sgr than is provided by the other dSphs, even though Sgr morphologically resembles the other dSphs now in terms of its more regular structure and lack of current star formation or gas. Sgr’s present morphological difference with the LMC is easily accounted for by the fact that the LMC, which apparently has just fallen into the MW environment for the first time (Kallivayalil et al. 2006; Besla et al. 2007; Piatek et al. 2008), has not experienced the tidal battering that the MW-bound Sgr has experienced for at least the past few Gyr. It is well known that severe tidal encounters such as has been experienced by Sgr can “tidally stir” dwarf irregular systems into dSphs (Mayer et al. 2001; Skillman et al. 2003; Klimentowski et al. 2007). Evidence that as recently as several Gyr ago Sgr was actively forming stars can be found in its color-magnitude diagram, which shows evidence for populations as young as 2 Gyr old or even younger (Sarajedini & Layden 1995; Layden & Sarajedini 2000; Siegel et al. 2007).

Typically SFRs and chemical enrichment are thought to be driven by the mass of a system. The mass-metallicity relation of dSphs has been investigated by, for example, Yoshii & Arimoto (1987) and Tamura et al. (2001), who find that metallicity is roughly logarithmically proportional to the mass of these satellite galaxies. Because Sgr is presently dominated by stellar populations with higher metallicity, that it is more massive than the other MW dSphs is consistent with the notion of a mass-metallicity relation. Curiously, however, Sgr is

more chemically evolved than the LMC, despite the fact that the mass of Sgr, at least that estimated the system had several Gyr ago by Paper IV of $\sim 2 - 5 \times 10^8 M_{\odot}$, is less than that of the LMC ($\sim 1 - 2 \times 10^{10} M_{\odot}$; Gardiner & Noguchi 1996; van der Marel et al. 2002). Certainly star formation efficiency may also be a significant driver in the rate of chemical evolution (Lanfranchi et al. 2006, 2007), but an expected consistency with mass-metallicity relations, and the possibility of a universal enrichment pattern (e.g., Fig. 10), may hint that Sgr was actually once significantly more massive than even the more recent, high estimates of its former mass, perhaps with a mass comparable to or larger than the LMC. If so, this would imply a much longer tidal stripping history for Sgr than has been previously observed (e.g., Paper I; Belokurov et al. 2006) and modeled (Paper IV; Fellhauer et al. 2006), perhaps with much of that mass lost as pure dark matter (to explain the lack of obvious stars from earlier orbits than has heretofore been observed).

6. Summary

Chemical abundances in stars are fossil records of the enrichment history of a galaxy and their distinctive patterns provide signatures that, if not uniquely branding its stars, at least allow us a means to test whether particular stars are likely to be associated with that system based on whether their chemistry fits into its overall abundance patterns. We have applied this test here not only to demonstrate the likely high purity of the spatially- and kinematically-selected sample of M giant Sgr tidal tail star candidates used in Paper V to show the existence of a strong metallicity gradient along the Sgr tails, but also to prove the likely Sgr-origin of the somewhat mysterious “North Galactic Cap moving group” also discussed in that previous contribution. We conclude that most of the NGC moving group stars are probably from the old trailing debris arm of Sgr (their MDF also supports this conclusion, see Paper V). Thus the present paper demonstrates the applicability of “chemical fingerprinting”, a technique long discussed as one of the potentially valuable future tools of stellar populations research.

The evolving chemical content of a galaxy depends on many variables — such as the stellar initial mass function and the SFR — that lead to the specific distribution of chemical patterns among the stars in the system. Tidal stripping can also shape the *observed* abundance patterns of the stars in a galaxy by preferentially removing certain populations, particularly if the system has spatial variations in metallicity and/or an age-metallicity relation over timescales overlapping the period during which the tidal loss of stars occurs. Both of these situations are at play in the Sgr system. Only by surveying both the stars lost from as well as remaining in a galaxy like Sgr do we have hope of recovering an unbiased view of

its chemical history. We have explored the chemical abundance patterns in stars along the Sgr tidal tails, which, when combined with data on stars in the Sgr core, afford us the most complete view of the original chemical abundance distributions of this system to date; but even then, our view here is likely to be rather incomplete and still tells us only part of the story. For example, we still do not have good information on the chemical properties of the oldest, most metal-poor Sgr populations.

In stars associated with Sgr we have found lower values of $[\text{Ti}/\text{Fe}]$ at $[\text{Fe}/\text{H}] > -1$ than for MW stars at the same $[\text{Fe}/\text{H}]$ (Fig. 3). And while the MW exhibits an apparent transition of $[\text{Ti}/\text{Fe}]$ to solar-like levels at $[\text{Fe}/\text{H}] \sim -0.7$, such a transition (and to even lower $[\text{Ti}/\text{Fe}]$ levels) happens for Sgr stars at $[\text{Fe}/\text{H}] \sim -1$. This shows that Sgr had a slower SFR than the MW, like other Galactic satellites. We also find the Sgr stars to have subsolar abundances of the light s-process element yttrium at all $[\text{Fe}/\text{H}]$ probed, while the heavy s-process element lanthanum is enhanced relative to the MW for $[\text{Fe}/\text{H}] \gtrsim -0.5$ (Figs. 4-6). This indicates the importance of low-metallicity AGB nucleosynthesis in the metal-rich Sgr stars (Smecker-Hane & McWilliam 2002) and is another signature of a slower SFR than occurred in the MW.

We also find that although the LMC and other dSphs exhibit similar chemical pattern trends as Sgr, these patterns exhibit their significant abundance transitions at lower $[\text{Fe}/\text{H}]$ than for Sgr. Such differences suggest a faster enrichment and more rapid star formation history in Sgr relative to those in the LMC and other dSphs. After applying a hypothetical shift in $[\text{Fe}/\text{H}]$ of +1 dex in the abundance patterns of other dSphs and +0.4 dex for the LMC we find that the chemical patterns of Sgr, LMC and other dSphs strongly resemble each other (Fig. 10), which suggests the possibility of a universal chemical enrichment progression among MW satellites that differs only by the SFRs; these SFRs, in turn, are likely correlated to the original masses of these systems. The relative shifts suggest that the relative SFR of these galaxies are, in order from slowest to fastest: the other MW dSphs, the LMC, Sgr and the MW respectively. Based on their close chemical similarities we suggest that Sgr was probably formerly more similar in nature to the present morphology and structure of the LMC than to those of other MW dSphs. The wide ranges of metallicities in Sgr suggests a large age spread, and implies a long duration of star formation in its central regions (Smecker-Hane & McWilliam 2002). This agrees with the discovery of quite young populations in the Sgr core (Siegel et al. 2007), which shows that Sgr has had even relatively recent star formation activity, like the LMC.

The color-magnitude distribution of Sgr stars demonstrates that its star formation history was highly variable, including some fairly well-defined “bursts” (Layden & Sarajedini 2000; Bellazzini et al. 1999; Monaco et al. 2002; Siegel et al. 2007). These produced popu-

lations with different, but overlapping radial density profiles in the progenitor satellite, and likely a strong internal metallicity gradient. In Paper V we found a strong metallicity gradient along the Sgr tidal arms, with the stars in these arms increasingly more metal-poor with angular separation (i.e. orbital phase difference) from the core. By comparing this gradient to models of the timescale for the disruption that produced these tails (Paper IV) we argued in Paper V that Sgr must have experienced a quite rapid change in its binding energy over the past several Gyr, even if the Sgr progenitor had one of the steepest metallicity gradients among the known MW dSphs. These multiple population bursts also created Sgr’s unique chemical patterns, especially at higher metallicities, compared to those of the MW (as well as to those of other dSphs). Nevertheless, while the abundance patterns of stars presently in the Sgr core differ greatly from those of MW stars of the same metallicity, in this paper we have found that the more metal-poor stars in the Sgr tail actually have abundance patterns that more closely resemble those of MW stars at their respective $[\text{Fe}/\text{H}]$. The Sgr example vividly demonstrates that while the current populations of stars in dSph satellites are indeed chemically differentiated from the MW field population and that “one could not build the MW halo from the *present* MW satellites” (as emphasized by, e.g., Unavane et al. 1996), this point is not very relevant because it is still possible that the MW halo field population could have derived from the *stripped off* populations of these very same satellites. Majewski et al. (2002) and Muñoz et al. (2006) have previously made the same point using the Carina dSph example.

The Sgr system can be seen as an evolutionary bridge from dSphs to the MW in galaxy evolution. On the one hand, recent models (Robertson et al. 2005; Font et al. 2006a,b) predict that the local halo assembled rapidly — before SN Ia had time to occur — with the early accretion and dissipation of a few massive satellites to produce the high values of $[\alpha/\text{Fe}]$ at low $[\text{Fe}/\text{H}]$ seen among halo field stars. Font et al. suggest the MW satellites accreted ~ 9 Gyr ago have all been disrupted completely, while the surviving satellites of today were only recently accreted into the MW system within the past few Gyr on relatively circular orbits. The implication is that these satellite systems have yet to contribute stars to the halo. On the other hand, Sgr clearly provides an example of an ongoing merger event that is not only contributing stars to the halo, but some low metallicity stars of high $[\alpha/\text{Fe}]$; it may therefore be seen as a counterexample to the “early accretion” hypothesis. However, Font et al. point out that none of the present MW satellites are presently located in the inner halo except Sgr and because of this Sgr may be an exceptional case. But the recent work on the Ursa Minor (Muñoz et al. 2005), Leo I (Sohn et al. 2007; Mateo et al. 2008) and Carina dSphs (Muñoz et al. 2006, 2008) yielding evidence for tidally stripped stars from these systems suggests that the present satellites may also have already contributed stars to the MW halo. This, coupled with the finding that some of the MW dSph stars at the lowest

metallicities are indeed α -enhanced (Shetrone et al. 2003; Geisler et al. 2005; Tolstoy 2005), suggests that Sgr may not be the only current contributor of such stars; at the very least these systems are likely to be *future* contributors of these stars, which shows that they did not all originate in early accretions.

The results of this paper would be considerably strengthened by a careful survey of the chemical abundance patterns of Sgr trailing arm stars. The significant overlap in orbital phase position along the Sgr leading arm (see Fig. 1 in Paper IV) “fuzzes out” the resolution of the dynamical stripping time. In contrast to the stronger phase mixing in the leading arm, the dynamics of the longer trailing arm demonstrate much better energy sorting of the debris, so that position along the trailing tail is much better correlated to the amount of time since a star was stripped from the Sgr core. Further scrutiny of cleanly isolated trailing arm stars may reveal even more clear chemical trends with dynamical age. We will investigate this in future work.

M.-Y.C. and S.R.M. acknowledge support from NSF grants AST-0307851 and AST-0807945. This project was also supported by the *SIM Lite* key project *Taking Measure of the Milky Way* under NASA/JPL contract 1228235. VVS and KC also thank support from the NSF via grant AST-0646790. D.G. gratefully acknowledges support from the Chilean *Centro de Astrofísica* FONDAF No. 15010003 and the Chilean *Centro de Excelencia en Astrofísica y Tecnologías Afines* (CATA).

REFERENCES

- Abadi, M. G., Navarro, J. F., & Steinmetz, M. 2006, *MNRAS*, 365, 747
- An, D., et al. 2009, *ApJ*, accepted
- Asplund, M., Grevesse, N., & Sauval, A. J. 2005, *ASP Conf. Ser.* 336: *Cosmic Abundances as Records of Stellar Evolution and Nucleosynthesis in honor of David L. Lambert*, 336, 25
- Bassino, L. P., & Muzzio, J. C. 1995, *The Observatory*, 115, 256
- Bell, E. F., et al. 2008, *ApJ*, 680, 295
- Bellazzini, M., Ferraro, F. R., & Buonanno, R. 1999, *MNRAS*, 307, 619
- Bellazzini, M., Correnti, M., Ferraro, F. R., Monaco, L., & Montegriffo, P. 2006, *A&A*, 446, L1

- Belokurov, V., et al. 2006, *ApJ*, 642, L137
- Besla, G., Kallivayalil, N., Hernquist, L., Robertson, B., Cox, T. J., van der Marel, R. P., & Alcock, C. 2007, *ApJ*, 668, 949
- Bonifacio, P., Sbordone, L., Marconi, G., Pasquini, L., & Hill, V. 2004, *A&A*, 414, 503
- Brown, J. A., Wallerstein, G., & Gonzalez, G. 1999, *AJ*, 118, 1245
- Bullock, J. S., & Johnston, K. V. 2005, *ApJ*, 635, 931
- Busso, M., Gallino, R., & Wasserburg, G. J. 1999, *ARA&A*, 37, 239
- Busso, M., Nucci, M. C., Chieffi, A., & Straniero, O. 2004, *Memorie della Societa Astronomica Italiana*, 75, 648
- Chou, M.-Y., et al. 2007, *ApJ*, 670, 346 (Paper V)
- Crane, J. D., Majewski, S. R., Rocha-Pinto, H. J., Frinchaboy, P. M., Skrutskie, M. F., & Law, D. R. 2003, *ApJ*, 594, L119
- Da Costa, G. S., & Armandroff, T. E. 1995, *AJ*, 109, 2533
- De Silva, G. M., Freeman, K. C., Asplund, M., Bland-Hawthorn, J., Bessell, M. S., & Collet, R. 2007, *AJ*, 133, 1161
- D’Onghia, E., & Lake, G. 2008, *ApJ*, 686, L61
- Duffau, S., Zinn, R., Vivas, A. K., Carraro, G., Mendez, R. A., Winnick, R., & Gallart, C. 2006, *ApJ*, 636, L97
- Fellhauer, M., et al. 2006, *ApJ*, 651, 167
- Fenner, Y., Gibson, B. K., Gallino, R., & Lugaro, M. 2006, *ApJ*, 646, 184
- Font, A. S., Johnston, K. V., Bullock, J. S., & Robertson, B. E. 2006a, *ApJ*, 638, 585
- Font, A. S., Johnston, K. V., Bullock, J. S., & Robertson, B. E. 2006b, *ApJ*, 646, 886
- Freeman, K., & Bland-Hawthorn, J. 2002, *ARA&A*, 40, 487
- Fulbright, J. P. 2000, *AJ*, 120, 1841
- Fulbright, J. P. 2002, *AJ*, 123, 404
- Gardiner, L. T., & Noguchi, M. 1996, *MNRAS*, 278, 191

- Geisler, D., Smith, V. V., Wallerstein, G., Gonzalez, G., & Charbonnel, C. 2005, *AJ*, 129, 1428
- Geisler, D., Wallerstein, G., Smith, V. V., & Casetti-Dinescu, D. I. 2007, *PASP*, 119, 939
- Gibson, B. K. 2007, in *Stellar Populations as Building Blocks of Galaxies*, IAU Symposium 241, ed. A. Vazdekis & R. F. Peletier, 241, 161
- Gratton, R. G., & Sneden, C. 1994, *A&A*, 287, 927
- Houdashelt, M. L., Bell, R. A., Sweigart, A. V., & Wing, R. F. 2000, *AJ*, 119, 1424
- Ibata, R., Gilmore, G., Irwin, M. J. 1994, *Nature*, 370, 194
- Ibata, R., Lewis, G. F., Irwin, M., Totten, E., & Quinn, T. 2001, *ApJ*, 551, 294
- Jurić, M., et al. 2008, *ApJ*, 673, 864
- Johnson, J. A. 2002, *ApJS*, 139, 219
- Johnson, J. A., Ivans, I. I., & Stetson, P. B. 2006, *ApJ*, 640, 801
- Kallivayalil, N., van der Marel, R. P., Alcock, C., Axelrod, T., Cook, K. H., Drake, A. J., & Geha, M. 2006, *ApJ*, 638, 772
- Keller, S. C., da Costa, G. S. & Prior, S. L. 2009, *MNRAS*, 394, 1045
- Klimontowski, J., Łokas, E. L., Kazantzidis, S., Prada, F., Mayer, L., & Mamon, A. 2007, *MNRAS*, 378, 353
- Kovács, N. 1983, *A&A*, 120, 21
- Kravtsov, A. V., Gnedin, O. Y., & Klypin, A. A. 2004, *ApJ*, 609, 482
- Kurucz, R. L., Furenlid, I., Brault, J., & Testerman, L. 1984, *Solar flux atlas from 296 to 1300 nm (National Solar Observatory Atlas)*
- Kurucz, R. L. 1994, *Kurucz CD-ROM 19, Solar Abundance Model Atmospheres (Cambridge: SAO)*
- Lanfranchi, G. A., Matteucci, F., & Cescutti, G. 2006, *A&A*, 453, 67
- Lanfranchi, G. A., & Matteucci, F. 2007, *A&A*, 468, 927
- Law, D. R., Johnston, K. V., & Majewski, S. R. 2005, *ApJ*, 619, 807 (Paper IV)

- Lawler, J. E., Bonvallet, G., Sneden, C. 2001, *ApJ*, 556, 452
- Layden, A. C. 1994, *AJ*, 108, 1016
- Layden, A. C., & Sarajedini, A. 2000, *AJ*, 119, 1760
- Li, Y.-S., & Helmi, A. 2008, *MNRAS*, 385, 1365
- López-Corredoira, M., Momany, Y., Zaggia, S., & Cabrera-Lavers, A. 2007, *A&A*, 472, L47
- Majewski, S. R. 1993, *ARA&A*, 31, 575
- Majewski, S. R., Munn, J. A., & Hawley, S. L. 1996, *ApJ*, 459, L73
- Majewski, S. R., Ostheimer, J. C., Patterson, R. J., Kunkel, W. E., Johnston, K. V., & Geisler, D. 2000, *AJ*, 119, 760
- Majewski, S. R., et al. 2002, *ASP Conf. Ser.* 285: Modes of Star Formation and the Origin of Field Populations, 285, 199
- Majewski, S. R., Skrutskie, M. F., Weinberg, M. D., & Ostheimer, J. C. 2003, *ApJ*, 599, 1082 (Paper I)
- Majewski, S. R., et al. 2004, *AJ*, 128, 245 (Paper II)
- Marigo, P., Girardi, L., Bressan, A., Groenewegen, M. A. T., Silva, L., & Granato, G. L. 2008 *A&A*, 482, 883
- Martin, N. F., Ibata, R. A., Conn, B.C., Lewis, G. F., Bellazzini, M., Irwin M. J., & McConnachie, A. W. 2004b, *MNRAS*, 355, 33
- Martínez-Delgado, D., Peñarrubia, J., Jurić, M., Alfaro, E. J., & Ivezić, Z. 2007, *ApJ*, 660, 1264
- Mateo, M., Olszewski, E. W., & Walker, M. G. 2008, *ApJ*, 675, 201
- Mayer, L., Governato, F., Colpi, M., Moore, B., Quinn, T., Wadsley, J., Stadel, J., & Lake, G. 2001, *ApJ*, 559, 754
- McWilliam, A., & Rich, R. M. 1994, *ApJS*, 91, 749
- McWilliam & Smecker-Hane 2005, *ASP Conf. Ser.* 336: Cosmic Abundances as Records of Stellar Evolution and Nucleosynthesis in honor of David L. Lambert, 336, 221
- Metz, M., Kroupa, P., Theis, C., Hensler, G., & Jerjen, H. 2009, *ApJ*, 697, 269

- Momany, Y., Zaggia, S. R., Bonifacio, P., Piotto, G., De Angeli, F., Bedin, L. R., & Carraro, G. 2004, *A&A*, 421, L29
- Momany, Y., Zaggia, S., Gilmore, G., Piotto, G., Carraro, G., Bedin, L. R., & de Angeli, F. 2006, *A&A*, 451, 515
- Monaco, L., Ferraro, F. R., Bellazzini, M., & Pancino, E. 2002, *ApJ*, 578, 47
- Monaco, L., Bellazzini, M., Ferraro, F. R., & Pancino, E. 2005a, *MNRAS*, 356, 1396
- Monaco, L., et al. 2005b, *A&A*, 441, 141
- Monaco, L., et al. 2007, *A&A*, 464, 201
- Mucciarelli, A., Carretta, E., Origlia, L., & Ferraro, F. R. 2008, *AJ*, 136, 375
- Muñoz, R. R., et al. 2005, *ApJ*, 631, L137
- Muñoz, R. R., et al. 2006, *ApJ*, 649, 201
- Muñoz, R. R., Majewski, S. R., & Johnston, K. V. 2008, *ApJ*, 679, 346
- Newberg, H. J., et al. 2002, *ApJ*, 569, 245
- Newberg, H. J., Yanny, B., Cole, N., Beers, T. C., Re Fiorentin, P., Schneider, D. P., & Wilhelm, R. 2007, *ApJ*, 668, 221
- Piatek, S., Pryor, C., & Olszewski, E. W. 2008, *AJ*, 135, 1024
- Pompéia, L., et al. 2008, *A&A*, 480, 379
- Prior, S. L., Da Costa, G. S., Keller, S. C., & Murphy, S. J. 2009, *ApJ*, 691, 306
- Prior, S. L., Da Costa, G. S., & Keller, S. C. 2009b, *ApJ*, 704, 1327
- Reddy, B. E., Tomkin, J., Lambert, D. L., & Allende Prieto, C. 2003, *MNRAS*, 340, 304
- Robertson, B., Bullock, J. S., Font, A. S., Johnston, K. V., & Hernquist, L. 2005, *ApJ*, 632, 872
- Rocha-Pinto, H. J., Majewski, S. R., Skrutskie, M. F., & Crane, J. D. 2003, *ApJ*, 594, L115
- Rocha-Pinto, H. J., Majewski, S. R., Skrutskie, M. F., Crane, J. D., & Patterson, R. J. 2004, *ApJ*, 615, 732

- Sadakane, K., Arimoto, N., Ikuta, C., Aoki, W., Jablonka, P., & Tajitsu, A. 2004, PASJ, 56, 1041
- Sarajedini, A., & Layden, A. C. 1995, AJ, 109, 1086
- Sbordone, L., Bonifacio, P., Buonanno, R., Marconi, G., Monaco, L., & Zaggia, S. 2007, A&A, 465, 815
- Searle, L., & Zinn, R. 1978, ApJ, 225, 357
- Shetrone, M. D., Côté, P., & Sargent, W. L. W. 2001, ApJ, 548, 592
- Shetrone, M. D., Venn, K. A., Tolstoy, E., Primas, F., Hill, V., & Kaufer, A. 2003, AJ, 125, 684
- Shetrone, M. D. 2004, in Origin and Evolution of the Elements, from the Carnegie Observatories Centennial Symposia, Carnegie Observatories Astrophysics Series, ed. A. McWilliam & M. Rauch, 218
- Siegel, M. H., et al. 2007, ApJ, 667, L57
- Sirko, E., et al. 2004, AJ, 127, 899
- Skillman, E. D., Côté, S., & Miller, B. W. 2003, AJ, 125, 593
- Smecker-Hane, T. A., & McWilliam, A. 2002, astro-ph/0205411
- Smith, V. V., & Lambert, D. L. 1985, ApJ, 294, 326
- Smith, V. V., & Lambert, D. L. 1986, ApJ, 311, 343
- Smith, V. V., & Lambert, D. L. 1990, ApJS, 72, 387
- Smith, V. V., Suntzeff, N. B., Cunha, K., Gallino, R., Busso, M., Lambert, D. L., & Straniero, O. 2000, AJ, 119, 1239
- Smith, V. V., et al. 2002, AJ, 124, 3241
- Snedden, C. 1973 ApJ, 184, 839
- Sohn, S. T., et al. 2007, ApJ, 663, 960
- Starkenburger, E., et al. 2009, ApJ, 698, 567
- Tamura, N., Hirashita, H., & Takeuchi, T. T. 2001, ApJ, 552, L113

- Tolstoy, E., Venn, K. A., Shetrone, M., Primas, F., Hill, V., Kaufer, A., & Szeifert, T. 2003, *AJ*, 125, 707
- Tolstoy, E. 2005, in *Near-Field Cosmology with Dwarf Elliptical Galaxies*, ed. H. Jerjen & B. Binggeli (Cambridge: Cambridge Univ. Press), 118
- Unavane, M., Wyse, R. F. G., Gilmore, G. 1996, *MNRAS*, 278, 727
- van der Marel, R. P., Alves, D. R., Hardy, E., & Suntzeff, N. B. 2002, *AJ*, 124, 2639
- Venn, K. A., Irwin, M., Shetrone, M. D., Tout, C. A., Hill, V., & Tolstoy, E. 2004, *AJ*, 128, 1177
- Vivas, A. K., Jaffe, Y. L., Zinn, R., Winnick, R., Duffau, S., & Mateu, C. 2008, *AJ*, 136, 1645
- Woosley, S. E., & Weaver, T. A. 1995, *ApJS*, 101, 181
- Yanny, B., et al. 2009, *ApJ*, 700, 1282
- Yoshii, Y., & Arimoto, N. 1987, *A&A*, 188, 13
- Zaritsky, D., & Harris, J. 2004, *ApJ*, 604, 167

Table 1. Atomic Data for The Selected Lines

Ion	λ (\AA)	χ (eV)	gf
Ti I	7489.572	2.249	2.339E-01
	7496.120	2.240	8.770E-02
Y II	7450.320	1.740	1.202E-01
La II	7483.234	0.126	2.080E-04
	7483.237	0.126	4.160E-04
	7483.259	0.126	2.080E-04
	7483.262	0.126	4.160E-04
	7483.267	0.126	6.240E-04
	7483.304	0.126	4.160E-04
	7483.308	0.126	6.240E-04
	7483.315	0.126	8.320E-04
	7483.367	0.126	6.240E-04
	7483.374	0.126	8.320E-04
	7483.382	0.126	1.039E-03
	7483.449	0.126	8.320E-04
	7483.458	0.126	1.039E-03
	7483.468	0.126	1.247E-03
	7483.550	0.126	1.039E-03
	7483.561	0.126	1.247E-03
7483.573	0.126	1.455E-03	
7483.670	0.126	1.247E-03	
7483.682	0.126	1.455E-03	

Table 2. Equivalent Width Measurements

Star No.	Ti I 7489.572	Ti I 7496.120	Y II 7450.320
Sgr(core)			
1849222 – 293217	...	193.5	38.3
1853333 – 320146	14.1
1854283 – 295740	147.1	124.8	35.1
1855341 – 302055	134.0	95.8	38.9
1855556 – 293316	28.5
1902135 – 313030	64.9	49.7	34.8
Sgr (north leading arm)			
0919216 + 202305	105.8	91.0	12.0
0925364 + 213807	113.0	109.1	37.0
1034395 + 245206	121.5	66.8	72.0
1100516 + 130216	74.3	57.1	23.7
1101112 + 191311	117.9	84.3	32.0
1111493 + 063915	115.6	84.8	24.4
1112480 + 013211	112.0	91.0	40.0
1114573 – 215126	112.0	113.0	16.0
1116118 – 333057	39.0
1128316 – 031647	122.3	97.5	37.8
1135388 – 022602	132.1	113.5	24.7
1140226 – 192500	113.7	98.2	24.0
1208101 – 090753	113.3	84.8	18.8
1223590 – 073028	111.3	103.8	18.0
1224255 – 061852	121.0	89.2	33.8
1227367 – 031834	114.0	93.7	33.0
1236549 – 002941	126.1	108.6	36.0
1249078 + 084455	100.6	95.0	34.0
1318500 + 061112	92.3	78.8	22.0
1319368 – 000817	109.5	105.6	24.0
1330472 – 211847	113.0	84.2	24.0
1334532 + 042053	100.5	96.2	22.0
1348366 + 220101	99.1	75.4	19.8
1407060 + 063311	115.4	109.5	22.3
1411221 – 061013	106.9	104.2	26.0
1435018 + 070827	108.7	88.9	21.7
1450544 + 244357	74.0	54.9	20.0
1456137 + 151112	117.0	88.2	52.3
1512142 – 075250	100.8	77.5	26.0
1538472 + 494218	131.5	123.8	26.0
Sgr(south leading arm)			
2031334 – 324453	...	66.2	19.2
2037196 – 291738	131.6	111.1	19.0
2046335 – 283547	...	63.3	12.8
2050020 – 345336	99.6	79.5	24.3

Table 2—Continued

Star No.	Ti I	Ti I	Y II
	7489.572	7496.120	7450.320
2105585 – 275602	129.9	82.0	24.5
2114412 – 301256	126.4	100.2	40.8
2130445 – 210034	87.7	51.6	21.4
2135183 – 203457	167.0	134.6	35.5
2154471 – 224050	127.4	123.6	31.9
2226328 – 340408	53.7	38.8	20.5
NGP			
1033045 + 491604	89.4	60.4	44.4
1041479 + 294917	111.1	66.1	34.7
1051302 + 004400	92.0	67.5	23.4
1115376 + 000800	116.3	92.1	21.5
1214190 + 071358	49.9	42.3	13.0
1257013 + 260046	92.3	73.2	23.0
1343047 + 221636	102.5	75.0	24.0
1412161 + 294303	119.7	103.2	40.0
1424425 + 414932	111.1	100.6	24.0
1429456 + 230043	88.5	72.7	18.0
1513011 + 222640	73.6	69.0	22.0
1536502 + 580017	95.1	82.8	26.0
1545189 + 291310	64.5	53.9	13.0
Standard Stars			
Arcturus	74.2	52.9	27.9
β Peg	131.0	106.0	34.0
β And	120.7	103.0	47.7
ρ Per	127.7	111.4	40.4
HD146051(mike)	129.1	100.8	43.6
HD146051(kpno)	124.9	95.7	45.8

Table 3. Chemical Abundances for The Program Stars

Star No.	T_{eff} Houdashelt (K)	$\log g$ (dex)	ξ (km s^{-1})	A(Fe)	[Fe/H]	standard deviation	A(Ti)	[Ti/Fe]	standard deviation	A(Y)	[Y/Fe]	standard deviation	A(La)	[La/Fe]
Sun	7.45	4.90	2.21	1.13	...
Sgr(core)														
1849222 - 293217	3850	0.9	2.43	7.24	-0.21	0.10	5.54	0.85	...	1.70	-0.30	...	1.51	...
1853333 - 320146	3750	0.7	2.60	7.15	-0.30	0.14	CR ^a	1.10	-0.81	...	1.38	...
1854283 - 295740	3750	0.0(-)	3.21	6.48	-0.97	0.06	4.20	0.27	0.17	0.98	-0.26	...	0.65	...
1855341 - 302055	3800	1.0	1.84	7.47	0.02	0.08	4.66	-0.32	0.09	1.89	-0.34	...	1.36	...
1855556 - 293316	3700	0.5	2.36	7.18	-0.27	0.07	CR ^a	1.37	-0.57	...	1.37	...
1902135 - 313030	3750	0.0(-)	1.04	6.41	-1.04	0.11	3.80	-0.06	0.10	1.18	0.01	...	CR ^a	...
Sgr (north leading arm)														
0919216 + 202305	3700	0.25	1.47	6.82	-0.63	0.08	4.29	0.02	0.12	0.75	-0.83	0.06	0.14	...
0925364 + 213807	3600	0.5	1.29	7.22	-0.23	0.07	4.70	0.03	0.24	1.76	-0.22	0.07	CR ^a	...
1034395 + 245206	3700	0.25	1.45	6.80	-0.65	0.09	4.25	0.00	0.33	2.08	0.52	0.12	CR ^a	...
1100516 + 130216	3800	0.0	1.35	6.39	-1.06	0.08	3.93	0.09	0.11	0.82	-0.33	0.13	0.06	...
1101112 + 191311	3700	0.8	1.51	7.47	0.02	0.09	4.53	-0.39	0.11	1.78	-0.45	0.09	1.15	...
1111493 + 063915	3600	0.0(-)	1.71	6.75	-0.70	0.09	4.08	-0.12	0.02	1.03	-0.48	...	0.05	...
1112480 + 013211	3800	0.5	1.60	6.97	-0.48	0.12	4.42	0.00	0.07	1.55	-0.18	0.02	0.44	...
1114573 - 215126	3550	0.0(-)	1.33	6.64	-0.81	0.07	4.42	0.33	0.30	0.81	-0.59	0.05	CR ^a	...
1116118 - 333057	3650	0.0(-)	1.39	6.32	-1.13	0.05	CR ^a	0.19	0.19	...	CR ^a	...
1128316 - 031647	3700	0.9	1.64	7.41	-0.04	0.05	4.61	-0.25	0.01	1.90	-0.27	...	1.10	...
1135388 - 022602	3700	0.9	1.23	7.45	0.00	0.07	5.15	0.25	0.02	1.66	-0.55	...	0.75	...
1140226 - 192500	3800	0.6	1.16	7.07	-0.38	0.05	4.78	0.26	0.08	1.31	-0.52	0.08	0.53	...
1208101 - 090753	3750	0.0(-)	1.82	6.46	-0.99	0.07	4.16	0.25	0.04	0.69	-0.53	...	-0.16	...
1223590 - 073028	3600	0.0	1.50	6.73	-0.72	0.08	4.29	0.11	0.20	0.88	-0.61	0.02	CR ^a	...
1224255 - 061852	3750	0.3	1.71	6.80	-0.65	0.08	4.33	0.08	0.03	1.30	-0.26	...	0.19	...
1227367 - 031834	3850	0.5	1.68	6.90	-0.55	0.08	4.47	0.12	0.09	1.36	-0.30	0.02	0.37	...
1236549 - 002941	3750	0.5	1.33	7.06	-0.39	0.10	4.80	0.29	0.05	1.53	-0.28	0.03	CR ^a	...
1249078 + 084455	3800	0.3	1.52	6.78	-0.67	0.10	4.37	0.14	0.22	1.31	-0.23	0.13	0.38 ^b	...
1318500 + 061112	3850	0.4	1.67	6.68	-0.77	0.10	4.21	0.08	0.16	1.01	-0.43	0.14	CR ^a	...
1319368 - 000817	3500	0.0(-)	1.64	6.86	-0.59	0.08	4.16	-0.15	0.25	1.09	-0.53	0.02	CR ^a	...
1330472 - 211847	3850	0.0(-)	1.75	6.35	-1.10	0.08	4.34	0.54	0.03	0.76	-0.35	0.09	CR ^a	...
1334532 + 042053	3700	0.25	1.49	6.83	-0.62	0.06	4.28	0.00	0.24	1.05	-0.54	0.15	0.29	...
1348366 + 220101	3800	0.1	1.49	6.63	-0.82	0.09	4.20	0.12	0.05	0.80	-0.59	...	-0.01	...
1407060 + 063311	3700	0.0(-)	1.78	6.50	-0.95	0.09	4.29	0.34	0.23	0.84	-0.42	...	-0.06	...
1411221 - 061013	3700	0.25	1.51	6.89	-0.56	0.06	4.38	0.04	0.26	1.18	-0.47	0.04	0.10	...
1435018 + 070827	3700	0.0(-)	1.61	6.53	-0.92	0.09	4.18	0.20	0.09	0.83	-0.46	...	-0.19	...
1450544 + 244357	3800	0.0	1.63	6.37	-1.08	0.08	3.86	0.04	0.11	0.70	-0.43	0.19	-0.10	...
1456137 + 151112	3750	0.0(-)	1.71	6.47	-0.98	0.08	4.26	0.34	0.02	1.38	0.15	...	-0.07	...
1512142 - 075250	3700	0.0(-)	1.26	6.48	-0.97	0.08	4.19	0.26	0.01	0.97	-0.27	...	CR ^a	...
1538472 + 494218	3600	0.0(-)	1.52	6.39	-1.06	0.08	4.55	0.71	0.20	0.99	-0.16	0.01	-0.20	...
Sgr(south leading arm)														
2031334 - 324453	3800	0.0(-)	2.67	6.13	-1.32	0.11	3.97	0.39	...	0.54	-0.35	...	CR ^a	...
2037196 - 291738	3700	0.0	2.32	6.75	-0.70	0.09	4.21	0.01	0.14	0.79	-0.72	...	0.39	...

Table 3—Continued

Star No.	T_{eff} Houdashelt (K)	$\log g$ (dex)	ξ (km s^{-1})	A(Fe)	[Fe/H]	standard deviation	A(Ti)	[Ti/Fe]	standard deviation	A(Y)	[Y/Fe]	standard deviation	A(La)	[La/Fe]
2046335 – 283547	3750	0.0(-)	2.56	6.19	-1.26	0.06	3.86	0.22	...	0.42	-0.53	...	CR ^a	...
2050020 – 345336	3800	0.0(-)	2.12	6.41	-1.04	0.10	4.06	0.20	0.14	0.79	-0.38	...	-0.04	-0.1
2105585 – 275602	3700	0.0(-)	2.13	6.49	-0.96	0.10	4.09	0.15	0.08	0.87	-0.38	...	CR ^a	...
2114412 – 301256	3750	0.0(-)	2.06	6.30	-1.15	0.10	4.25	0.50	0.08	1.12	0.06	...	0.21	0.2
2130445 – 210034	3750	0.0(-)	2.62	6.10	-1.35	0.10	3.71	0.16	0.04	0.63	-0.23	...	0.04	0.2
2135183 – 203457	3700	0.0(-)	2.30	6.55	-0.90	0.13	4.52	0.52	0.3	1.08	-0.23	...	0.04	-0.1
2154471 – 224050	3800	0.1	2.14	6.54	-0.91	0.06	4.44	0.45	0.26	1.00	-0.30	...	0.19	-0.0
2226328 – 340408	3800	0.0(-)	1.93	6.11	-1.34	0.09	3.58	0.02	0.15	0.61	-0.26	...	-0.47	-0.2
NGP														
1033045 + 491604	3800	0.3	1.56	6.70	-0.75	0.09	4.01	-0.14	0.00	1.47	0.01	0.14	0.46	0.0
1041479 + 294917	3800	0.0(-)	1.56	6.21	-1.24	0.10	4.20	0.54	0.15	1.01	0.04	...	0.04	0.1
1051302 + 004400	3800	0.0(-)	1.65	6.07	-1.38	0.06	4.05	0.53	0.06	0.70	-0.13	...	-0.32	-0.0
1115376 + 000800	3800	0.0	1.56	6.49	-0.96	0.10	4.42	0.48	0.04	0.76	-0.49	...	-0.06	-0.2
1214190 + 071358	3750	0.0(-)	1.73	6.32	-1.13	0.10	3.51	-0.26	0.21	0.45	-0.63	0.18	CR ^a	...
1257013 + 260046	3750	0.0(-)	1.68	6.49	-0.96	0.09	4.01	0.07	0.11	0.81	-0.44	0.22	0.01	-0.1
1343047 + 221636	3750	0.0(-)	2.26	6.37	-1.08	0.10	3.94	0.12	0.09	0.81	-0.32	0.02	-0.03	-0.0
1412161 + 294303	3800	0.6	1.76	7.02	-0.43	0.07	4.50	0.03	0.12	1.59	-0.19	0.05	0.49	-0.2
1424425 + 414932	3700	0.1	1.59	6.73	-0.72	0.07	4.31	0.13	0.17	1.01	-0.48	0.06	0.10	-0.3
1429456 + 230043	3750	0.0(-)	1.88	6.48	-0.97	0.11	3.93	0.00	0.16	0.66	-0.58	0.09	0.04	-0.1
1513011 + 222640	3700	0.0(-)	1.17	6.60	-0.85	0.10	3.94	-0.11	0.24	0.91	-0.45	0.08	-0.12 ^c	-0.4
1536502 + 580017	3750	0.0(-)	1.53	6.61	-0.84	0.10	4.14	0.08	0.17	0.94	-0.43	0.08	-0.07	-0.3
1545189 + 291310	3850	0.1	1.52	6.45	-1.00	0.09	3.96	0.06	0.07	0.51	-0.70	0.04	-0.18	-0.3
Standard Stars														
Arcturus	4250	1.4	1.66	6.74	-0.71	0.10	4.54	0.35	0.07	1.44	-0.06	0.09	0.34	-0.0
β Peg	3750	0.6	1.73	6.98	-0.47	0.08	4.59	0.16	0.02	1.54	-0.20	0.02	0.57	-0.0
β And	3850	0.9	1.96	7.12	-0.33	0.06	4.55	-0.02	0.12	1.89	0.01	0.00	0.79	-0.0
ρ Per	3650	0.7	1.35	7.36	-0.09	0.15	4.93	0.12	0.06	1.97	-0.15	0.10	0.86	-0.1
HD146051(mike)	4000	1.0	2.07	6.98	-0.47	0.08	4.70	0.27	0.05	1.69	-0.05	...	0.75	0.0
HD146051(kpno)	4000	1.0	1.81	7.06	-0.39	0.08	4.74	0.23	0.01	1.76	-0.06	0.06	0.80	0.0
HD146051 (average)	4000	1.0	...	7.02	-0.43	...	4.72	0.25	...	1.73	-0.06	...	0.78	0.0

^a Lines unmeasurable due to cosmic rays or other defects are marked "CR".

^b Measurement uncertain due to spectrum defect on the blue edge of the observed La line.

^c Measurement uncertain due to unusual shape of the observed La line.

^d Larger measurement uncertainty of La due to noisier spectrum. These measurements were excluded from the figures.

Table 4. Comparison of The Control Sample Stars with References

Star Name Reference	T_{eff} (K)	$\log g$ (dex)	ξ (km s^{-1})	A(Fe)	A(Ti)	A(Y)	A(La)
<i>Arcturus</i>							
This Work	4250	1.4	1.66	6.74 ± 0.10	4.54 ± 0.07	1.44 ± 0.09	0.34 ± 0.07
McWilliam & Rich 1994	4280	1.3	1.4	6.98 ± 0.18	4.77 ± 0.13	1.28 ± 0.30	0.53 ± 0.01
Smith et al. 2000	4300	1.7	1.6	6.78 ± 0.11	4.64 ± 0.12	1.4 ± 0.15	0.62
<i>β Peg</i>							
This Work	3750	0.6	1.73	6.98 ± 0.08	4.59 ± 0.02	1.54 ± 0.02	0.57 ± 0.01
Smith & Lambert 1985 ^a	3600	1.2	2.0	7.41 ± 0.13	4.87 ± 0.10	2.19	...
This Work with S&L Parameters	3600	1.2	2.0	7.32 ± 0.10	4.59 ± 0.04	2.00 ± 0.02	...
<i>β And</i>							
This Work	3850	0.9	1.96	7.12 ± 0.06	4.55 ± 0.12	1.89 ± 0.01	0.79 ± 0.02
Smith & Lambert 1985 ^a	3800	1.6	2.1	7.42 ± 0.11	4.87 ± 0.12	2.35	...
This Work with S&L Parameters	3800	1.6	2.1	7.38 ± 0.07	4.62 ± 0.13	2.29 ± 0.00	...
<i>ρ Per</i>							
This Work	3650	0.7	1.35	7.36 ± 0.15	4.93 ± 0.06	1.97 ± 0.10	0.86 ± 0.03
Smith & Lambert 1986 ^a	3500	0.8	1.8	7.57 ± 0.17	4.86 ± 0.14	2.00	...
This Work with S&L Parameters	3500	0.8	1.8	7.30 ± 0.20	4.58 ± 0.12	2.00 ± 0.09	...

^a $A(X)$ are derived using the relative abundance ratios $[X/H]$ in S&L and the absolute abundances of α Tau. The absolute abundances of α Tau are derived from the stellar parameters and the EWs in S&L, but with the Kurucz model atmospheres and the gf -values in this work.

Table 5. Sensitivity of Abundances to Stellar Parameters

Star Name Element	$\Delta T_{\text{eff}} = +100$ (K)	$\Delta \log g = +0.2$ (dex)	$\Delta \xi = +0.2$ (km s^{-1})
<i>β Peg</i>			
$\Delta A(\text{Fe})$	-0.06	+0.08	-0.09
$\Delta A(\text{Ti})$	+0.10	+0.03	-0.10
$\Delta A(\text{Y})$	-0.03	+0.09	-0.02
$\Delta A(\text{La})$	+0.03	+0.08	+0.00
<i>β And</i>			
$\Delta A(\text{Fe})$	-0.07	+0.07	-0.09
$\Delta A(\text{Ti})$	+0.10	+0.03	-0.08
$\Delta A(\text{Y})$	-0.04	+0.09	-0.02
$\Delta A(\text{La})$	+0.01	+0.08	-0.01
<i>ρ Per</i>			
$\Delta A(\text{Fe})$	-0.12	+0.06	-0.09
$\Delta A(\text{Ti})$	+0.04	+0.04	-0.15
$\Delta A(\text{Y})$	-0.07	+0.08	-0.04
$\Delta A(\text{La})$	+0.00	+0.09	+0.00

Table 6. Score Card for The Program Stars

Star No.	$N_\sigma([\text{Ti}/\text{Fe}])$	$N_\sigma([\text{Y}/\text{Fe}])$	$N_\sigma([\text{La}/\text{Fe}])$	Sum of Abs(N_σ)	Average of Abs(N_σ)
Sgr(core)					
1849222 – 293217	15.6	-2.3	7.8	25.7	8.6
1853333 – 320146	...	-5.7	6.8	12.5	6.3
1854283 – 295740	0.1	-1.4	5.1	6.6	2.2
1855341 – 302055	-5.5	-2.7	3.7	11.9	4.0
1855556 – 293316	...	-4.1	6.0	10.1	5.1
1902135 – 313030	-3.1	0.5	...	3.6	1.8
Sgr (north leading arm)					
0919216 + 202305	-0.9	-5.5	-1.9	8.3	2.8
0925364 + 213807	-0.3	-1.7	...	2.0	1.0
1034395 + 245206	-1.3	3.7	...	5.0	2.5
1100516 + 130216	-1.7	-1.8	0.5	4.0	1.3
1101112 + 191311	-6.8	-3.5	1.8	12.1	4.0
1111493 + 063915	-3.7	-3.1	-2.2	9.0	3.0
1112480 + 013211	-0.9	-1.2	-0.5	2.6	0.9
1114573 – 215126	0.6	-3.8	...	4.4	2.2
1116118 – 333057	...	1.8	...	1.8	1.8
1128316 – 031647	-4.4	-2.2	2.0	8.6	2.9
1135388 – 022602	5.0	-4.1	-1.3	10.4	3.5
1140226 – 192500	4.2	-3.6	-0.5	8.3	2.8
1208101 – 090753	-0.1	-3.2	-1.8	5.1	1.7
1223590 – 073028	-1.5	-4.0	...	5.5	2.8
1224255 – 061852	0.2	-1.6	-1.3	3.1	1.0
1227367 – 031834	1.2	-2.0	-0.4	3.6	1.2
1236549 – 002941	4.8	-2.0	...	6.8	3.4
1249078 + 084455	1.3	-1.4	0.5	3.2	1.1
1318500 + 061112	-1.8	-2.7	...	4.5	2.3
1319368 – 000817	-3.9	-3.5	...	7.4	3.7
1330472 – 211847	2.7	-1.9	...	4.6	2.3
1334532 + 042053	-1.2	-3.6	-0.7	5.5	1.8
1348366 + 220101	-1.4	-3.8	-1.8	7.0	2.3
1407060 + 063311	0.7	-2.5	-1.3	4.5	1.5
1411221 – 061013	-0.3	-3.1	-2.8	6.2	2.1
1435018 + 070827	-0.6	-2.8	-3.0	6.4	2.1
1450544 + 244357	-2.2	-2.5	-0.6	5.3	1.8
1456137 + 151112	0.7	1.4	-1.1	3.2	1.1
1512142 – 075250	0.0	-1.5	...	1.5	0.8
1538472 + 494218	4.3	-0.6	-1.6	6.5	2.2
Sgr(south leading arm)					
2031334 – 324453	1.2	-1.7	...	2.9	1.5
2037196 – 291738	-1.2	-4.7	0.8	6.7	2.2
2046335 – 283547	-0.4	-3.0	...	3.4	1.7
2050020 – 345336	-0.6	-2.2	-0.3	3.1	1.0

Table 6—Continued

Star No.	$N_\sigma([\text{Ti}/\text{Fe}])$	$N_\sigma([\text{Y}/\text{Fe}])$	$N_\sigma([\text{La}/\text{Fe}])$	Sum of Abs(N_σ)	Average of Abs(N_σ)
2105585 – 275602	-1.1	-2.2	...	3.3	1.7
2114412 – 301256	2.3	0.9	2.7	5.9	2.0
2130445 – 210034	-1.0	-0.9	2.7	4.6	1.5
2135183 – 203457	2.5	-1.2	-0.7	4.4	1.5
2154471 – 224050	1.8	-1.7	0.7	4.2	1.4
2226328 – 340408	-2.4	-1.1	-1.8	5.3	1.8
NGP					
1033045 + 491604	-3.9	0.3	1.8	6.1	2.0
1041479 + 294917	2.7	0.9	1.6	5.2	1.7
1051302 + 004400	2.6	-0.2	-1.5	4.3	1.4
1115376 + 000800	2.1	-3.0	-1.1	6.2	2.1
1214190 + 071358	-5.1	-3.8	...	8.9	4.5
1257013 + 260046	-1.9	-2.6	-0.5	5.0	1.7
1343047 + 221636	-1.4	-1.7	0.0	3.1	1.0
1412161 + 294303	-0.2	-1.3	-0.4	1.9	0.6
1424425 + 414932	-1.3	-3.1	-1.6	6.0	2.0
1429456 + 230043	-2.6	-3.6	-0.2	6.4	2.1
1513011 + 222640	-3.6	-2.8	-2.5	8.9	3.0
1536502 + 580017	-1.8	-2.7	-1.9	6.4	2.1
1545189 + 291310	-2.0	-4.4	-1.9	8.3	2.8

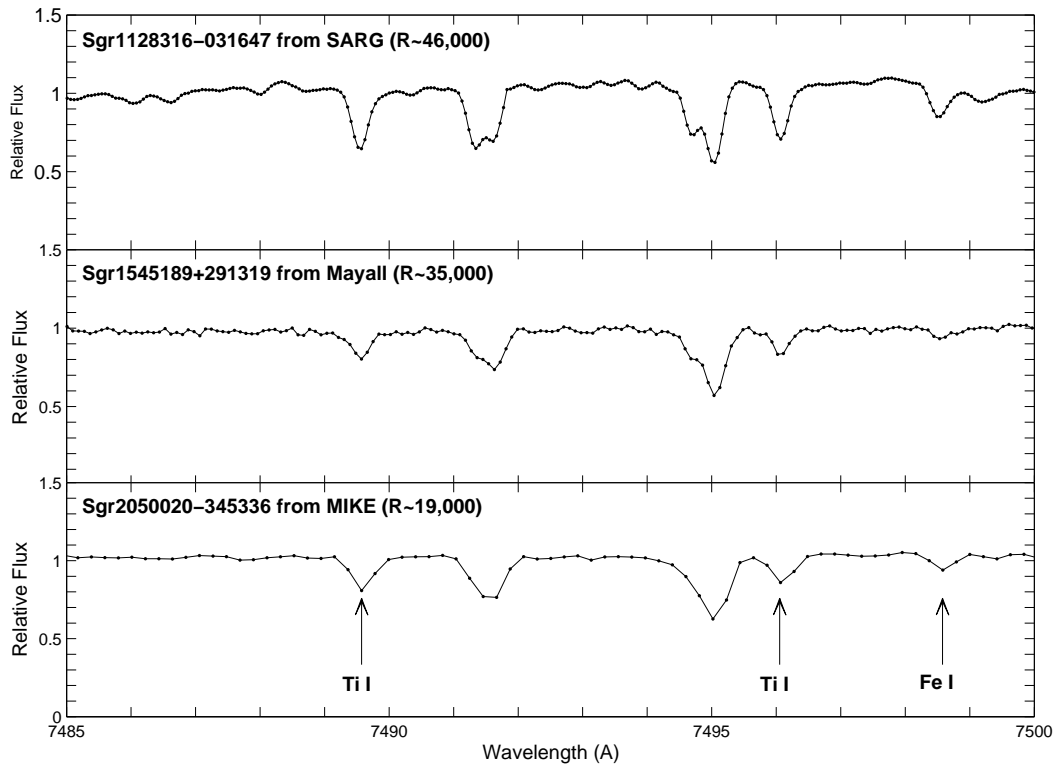


Fig. 1.— Sample spectra of three M giants from the three different spectrographs used in this study. Sample titanium and iron lines are identified in the figure.

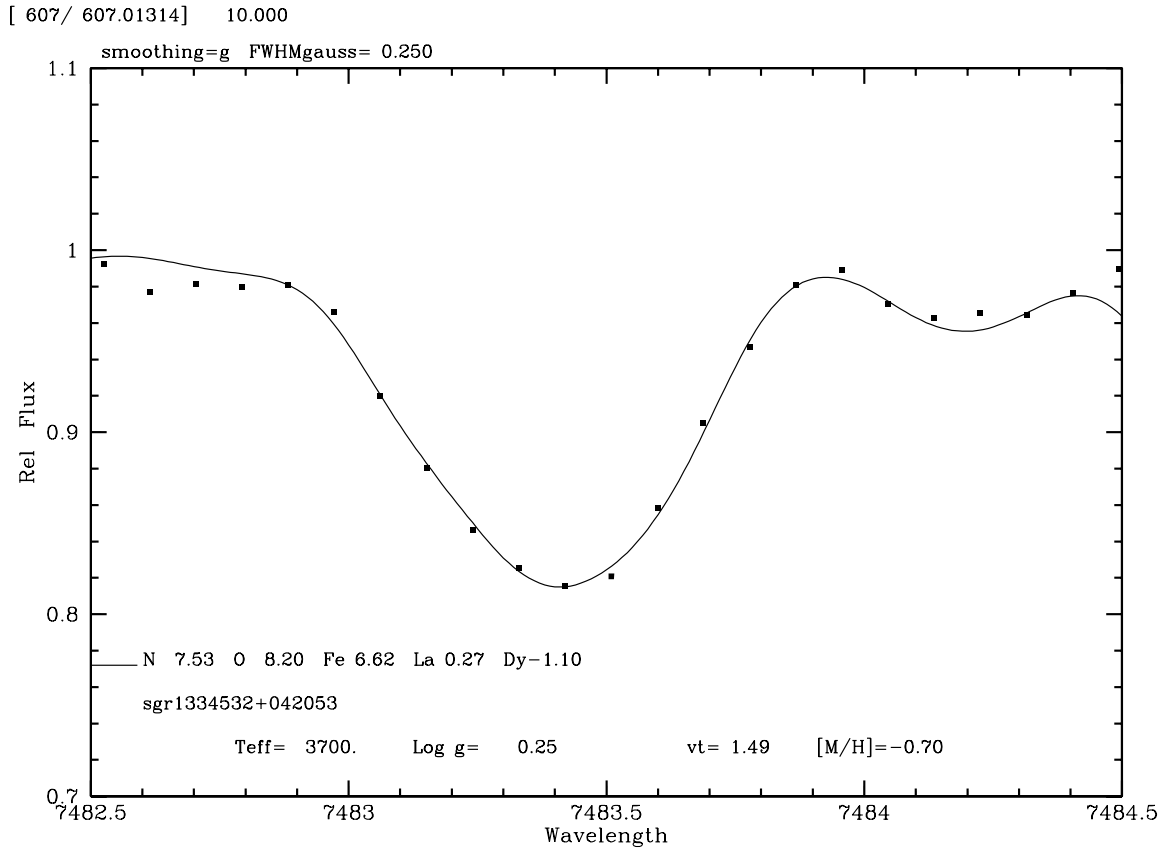


Fig. 2.— Sample observed (filled circles) and synthetic spectra (continuous curves) for the La II 7483.5 Å line in Sgr1334532+042053.

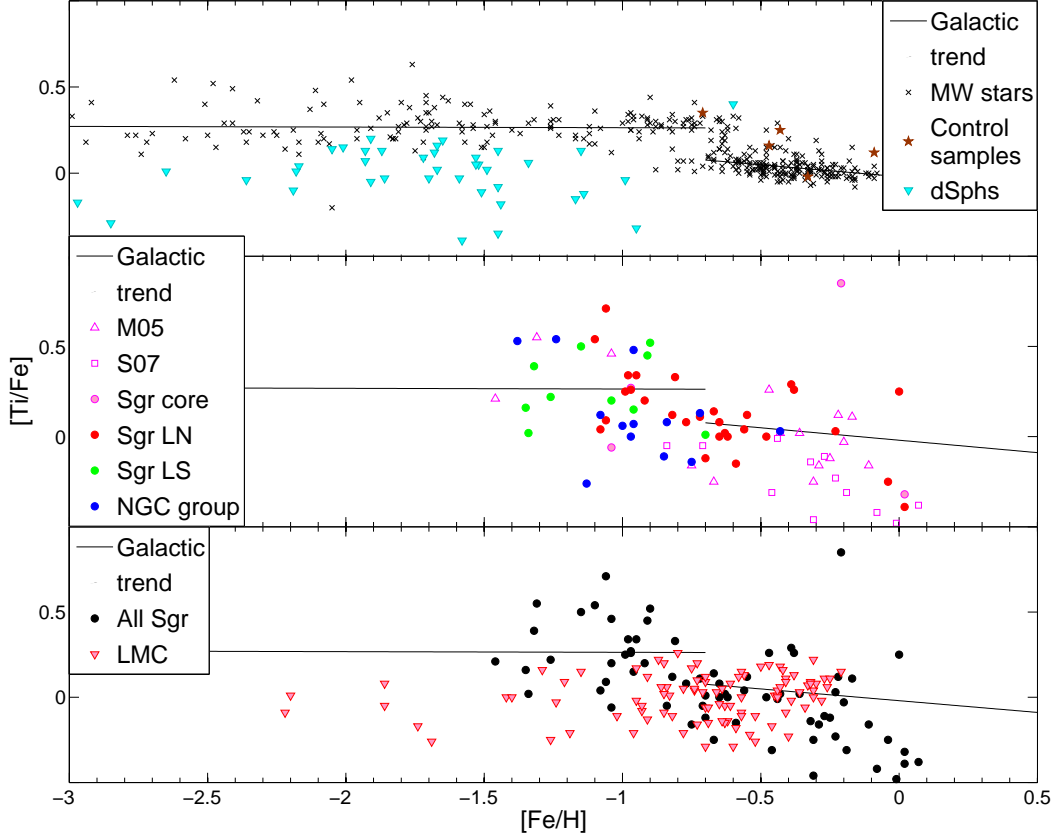


Fig. 3.— The distribution of $[\text{Ti}/\text{Fe}]$ as a function of $[\text{Fe}/\text{H}]$ for (*top panel*) Milky Way (black crosses) and dSph stars (cyan triangles). The MW data are from Fulbright (2000), Johnson (2002) and Reddy et al. (2003). The dSph data are from Shetrone et al. (2001; 2003), Sadakane et al. (2004) and Geisler et al. (2005). The brown star symbols show the “control sample” stars for our survey. The lines represent a two-piece linear fit to the MW star distribution, where separate fits are used to either side of the apparent transition at $[\text{Fe}/\text{H}] = -0.7$. (*middle panel*) Sgr stars with all stars in our spectroscopic sample shown as filled, colored circles: Sgr core (magenta), leading arm north (Sgr LN, red), leading arm south (Sgr LS, green) and the “NGC” group of stars having more positive GSR radial velocities that are well off the main leading arm velocity trend (blue). The open symbols show Sgr core stars from Monaco et al. (2005b, M05) and Sbordone et al. (2007, S07). (*bottom panel*) The pink triangles are LMC stars from Johnson et al. (2006), Pompéia et al. (2008) and Mucciarelli et al. (2008), to which we compare the Sgr stars from the middle panel, shown here as solid black circles.

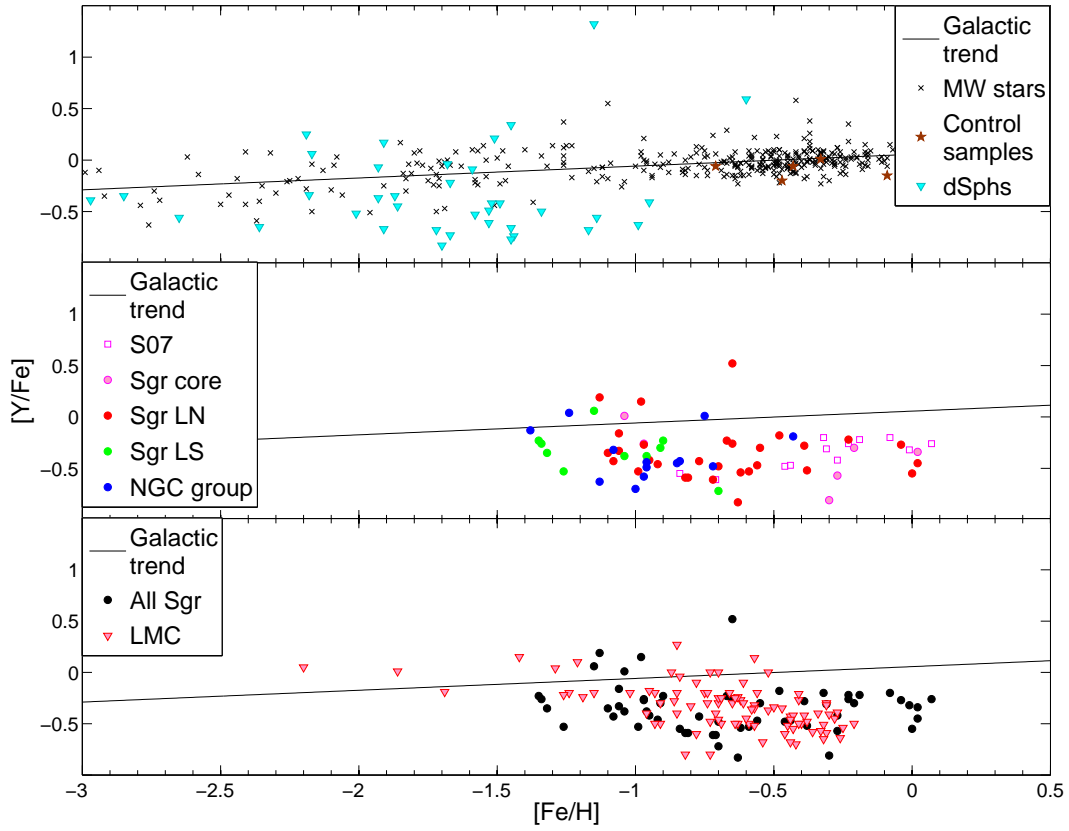


Fig. 4.— The same as Fig. 3, but for $[Y/Fe]$ versus $[Fe/H]$. The MW data are those published by Gratton & Sneden (1994), Fulbright (2000), Johnson (2002) and Reddy et al. (2003). Other data come from the same references as Fig. 3.

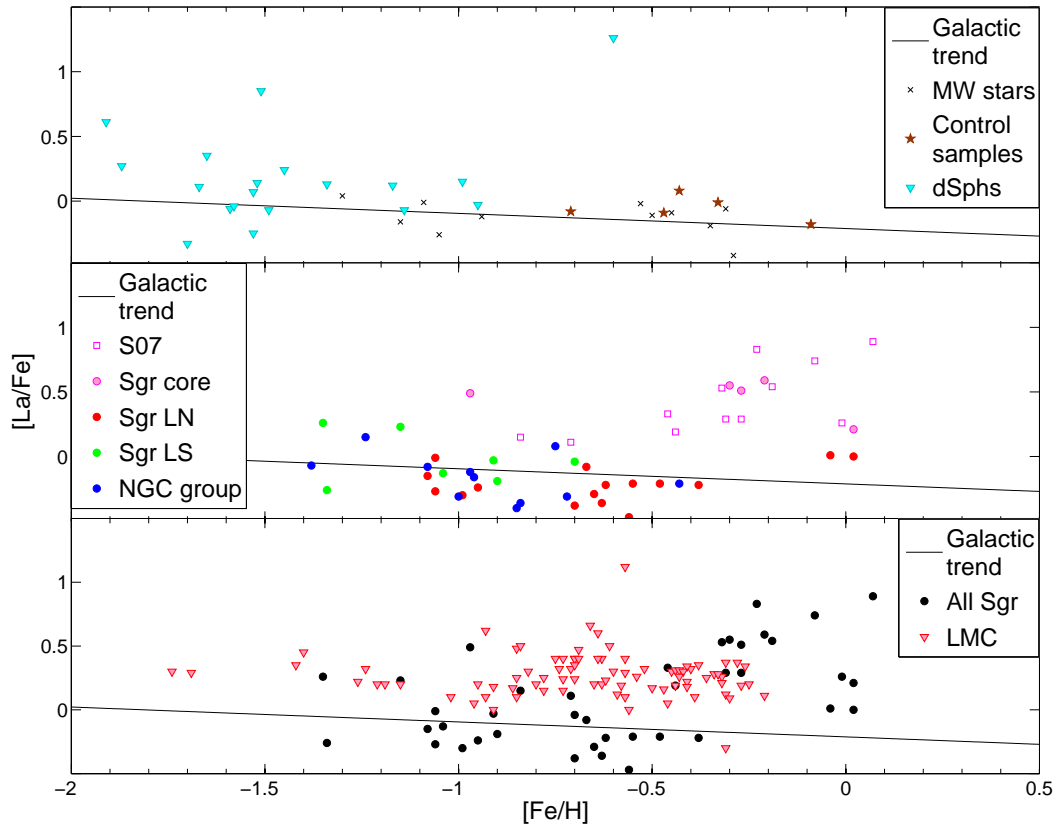


Fig. 5.— The same as Fig. 4, but for $[La/Fe]$ versus $[Fe/H]$. The data for Galactic stars come from Gratton & Sneden (1994), and for dSphs come from Shetrone et al. (2003), Sadakane et al. (2004) and Geisler et al. (2005). The LMC data come from the same references as Fig. 3.

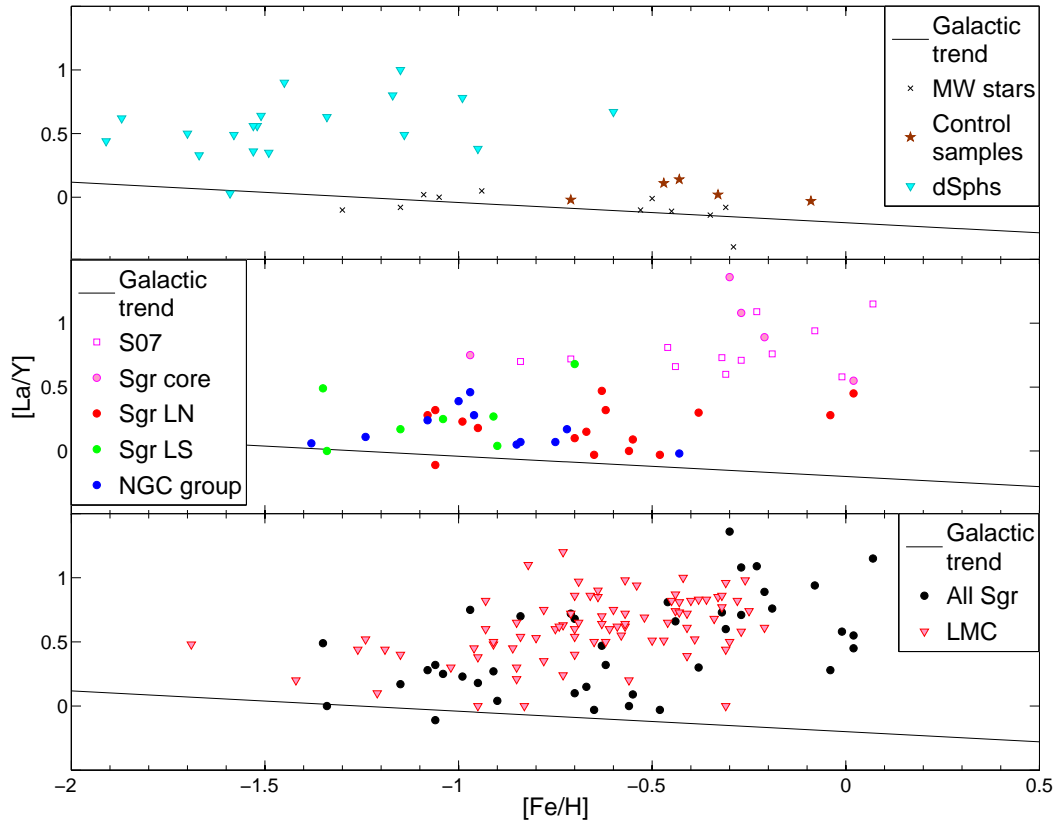


Fig. 6.— The same as Fig. 5, but for $[La/Y]$ versus $[Fe/H]$.

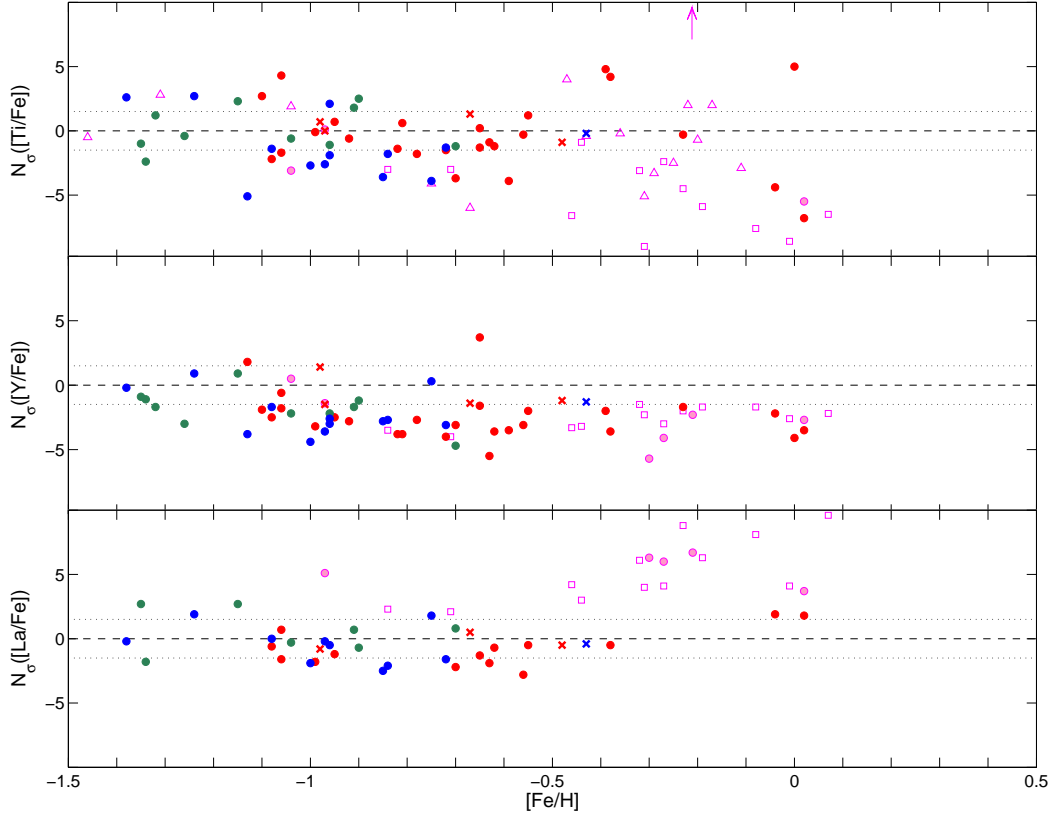


Fig. 7.— From top to bottom: $N_\sigma([Ti/Fe])$, $N_\sigma([Y/Fe])$ and $N_\sigma([La/Fe])$ versus $[Fe/H]$, showing the quantitative deviation trend for each subsample comparing with the Milky Way. The color coded as the previous figures, the open symbols are Sgr core stars from Monaco et al. (2005b) and Sbordone et al. (2007). The dashed lines represent zero σ , and dotted lines are $\pm 1.5\sigma$

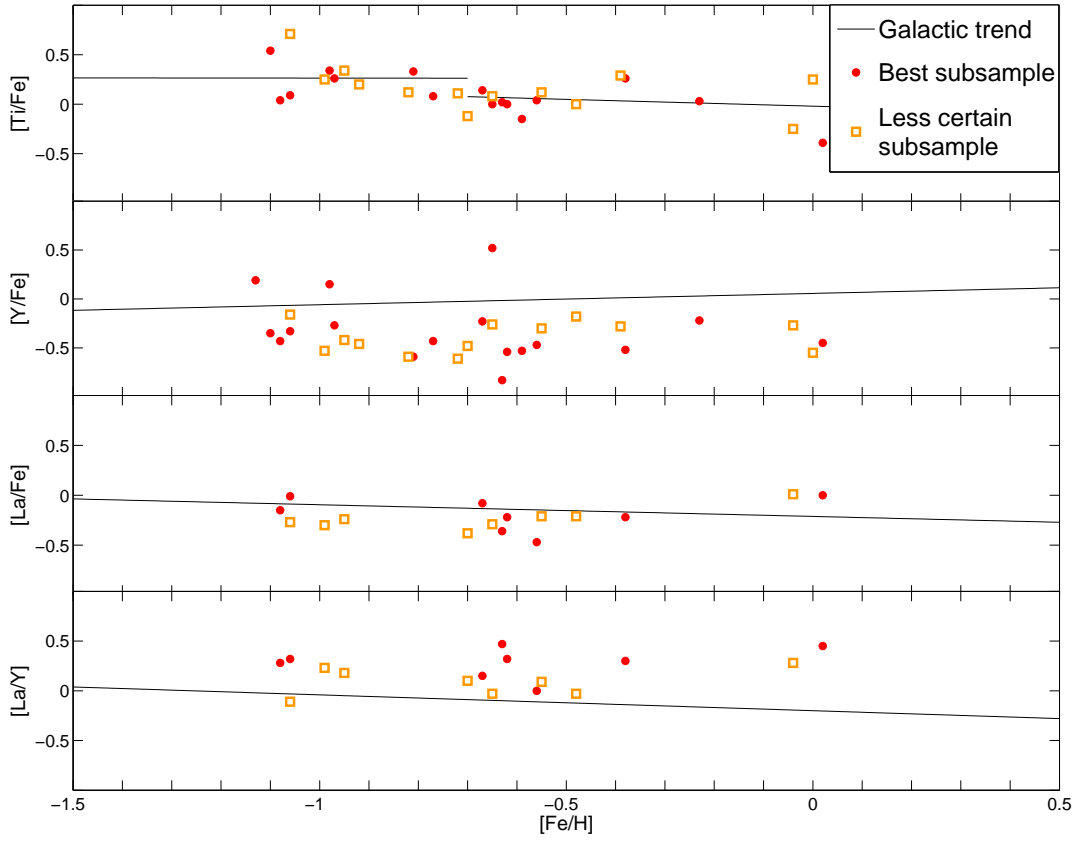


Fig. 8.— The distribution of $[Ti/Fe]$, $[Y/Fe]$, $[La/Fe]$ and $[La/Y]$ as a function of $[Fe/H]$ for the best and less certain Sgr LN groups.

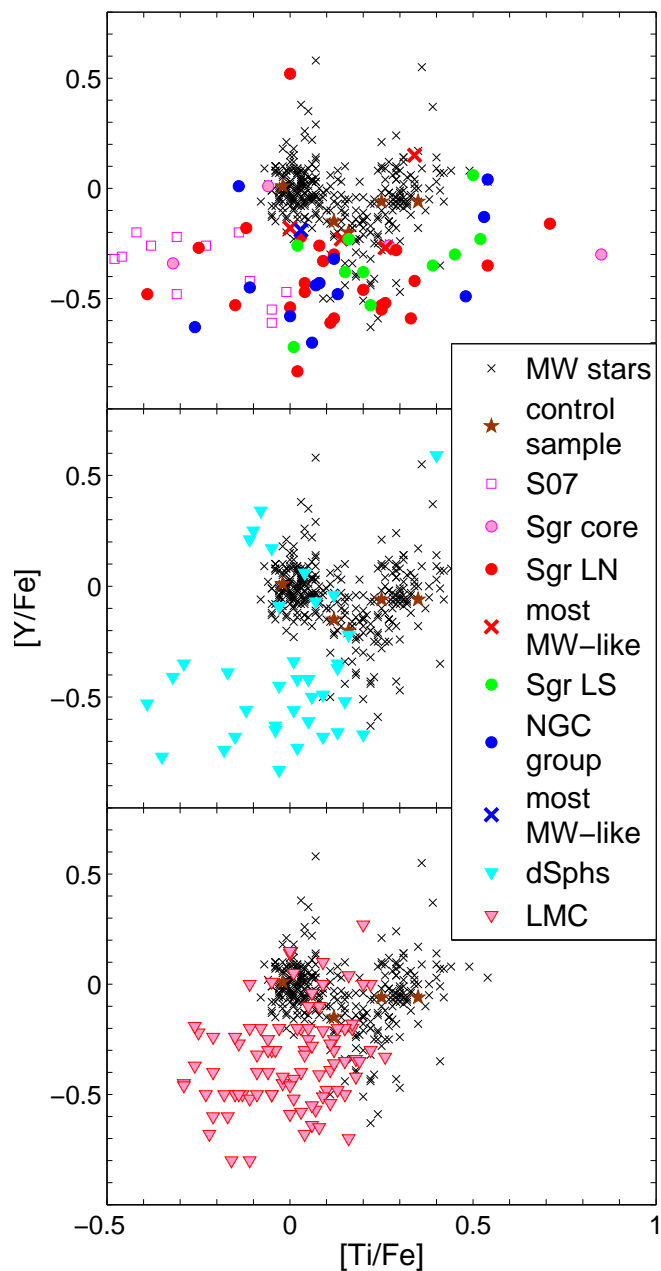


Fig. 9.— Distribution of $[Y/Fe]$ versus $[Ti/Fe]$ for our stars (*top panel*), stars in other dSphs (*middle panel*) and stars in the LMC (*bottom panel*) — with all stars color coded as in the previous figures — compared with Milky Way stars. The latter lie within a well-defined, V-shaped distribution near the top of each panel.

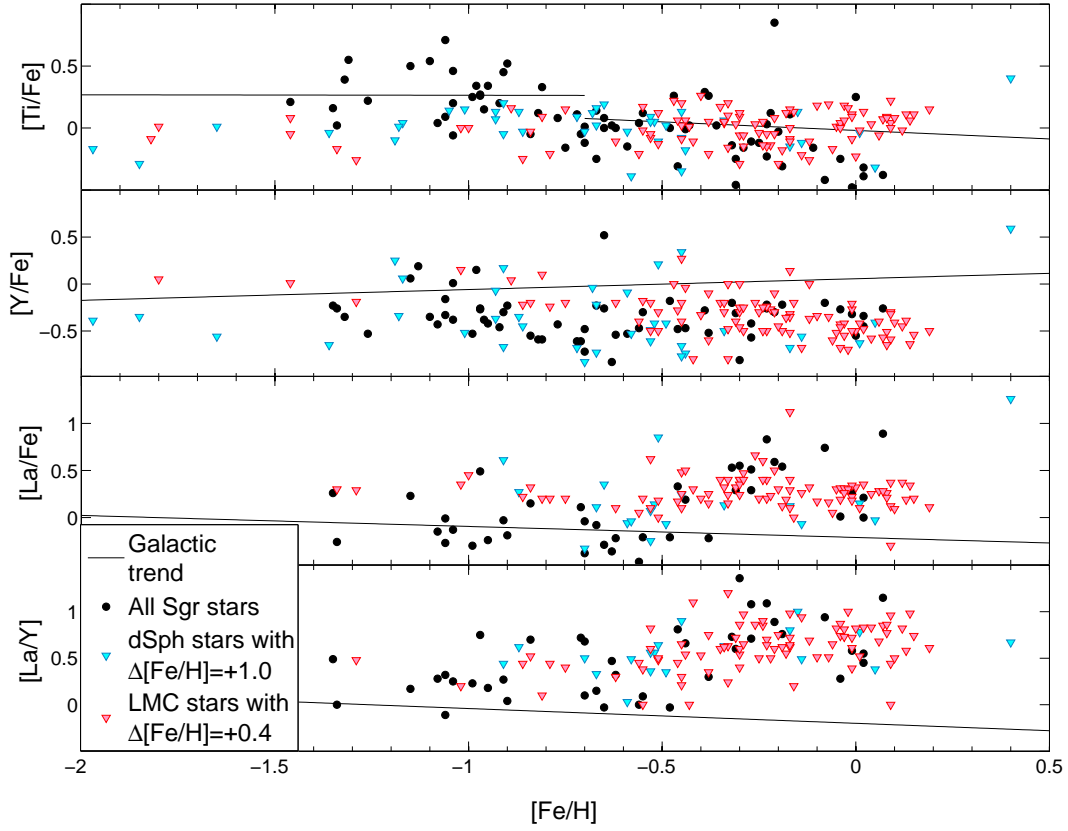


Fig. 10.— The distribution of $[Ti/Fe]$, $[Y/Fe]$, $[La/Fe]$ and $[La/Y]$ as a function of $[Fe/H]$ for Sgr, LMC and other dSphs, but with a shift of +0.4 dex in $[Fe/H]$ for LMC, and +1 dex in $[Fe/H]$ for other dSphs.